DAMAGE THRESHOLD STUDIES IN LASER CRYSTALS:

[illegible]

By

[illegible]

[illegible]

[illegible]

Contract No. F19628-69-C-0277

Project No. 8693

SEMI-ANNUAL REPORT NO. 2

JULY 1970

Contract Monitor C Martin Stickley
OPTICAL PHYSICS LABORATORY

Sponsored by
Advanced Research Projects Agency
ARPA Order No. 1434
Monitored by
AIR FORCE CAMBRIDGE RESEARCH LABORATORIES
AIR FORCE SYSTEMS COMMAND
UNITED STATES AIR FORCE
BEDFORD, MASSACHUSETTS 01730

[illegible]

[illegible]

Hughes Research Laboratories
Hughes Aircraft Company
3011 Malibu Canyon Road
Malibu, California 90265

Contract No. F19628-69-C-0277
Project No. 8691

Semi-Annual Report No. 2

July 1970

This document has been approved for public
Release and Sale; its distribution is unlimited.

Contract Monitor: C. Martin Stickley
Optical Physics Laboratory

Sponsored by
Advanced Research Projects Agency
ARPA Order No. 1434
Monitored by
AIR FORCE CAMBRIDGE RESEARCH LABORATORIES
AIR FORCE SYSTEMS COMMAND
UNITED STATES AIR FORCE
BEDFORD, MASSACHUSETTS 01730

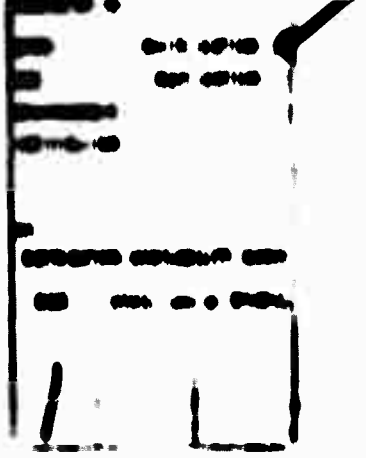

ABSTRACT

In this report the results of a number of experiments are presented as well as a summary of the theoretical work. Bulk damage thresholds for several ruby and sapphire samples from different sources are presented. The problem of surface damage is discussed, and qualitative comparisons between entrance and exit surface damage are made. Differences between the gross characteristics of bulk damage in ruby and sapphire are presented and discussed. The dependence of damage threshold on TiO_2 doping and optical pumping is presented. The unexpected results are discussed and further experiments proposed. The theoretical treatment deals with processes by which "cold" conduction electrons may damage the lattice before they gain enough energy to ionize their surroundings. It is shown that the energy that the conduction electrons absorb linearly from the optical beam is deposited almost immediately in the lattice and is of sufficient magnitude to form a rupturing shock wave. It is also shown that the photoexcitation of impurity levels is enhanced by the presence of conduction electrons. The presence of conduction electrons and excited impurities is likely to alter the refractive index significantly and affect the focusing (self- or external) in a complicated way. Implications of these results for raising damage thresholds are discussed.

TABLE OF CONTENTS

LIST OF ILLUSTRATIONS

I. EXPERIMENTAL STUDIES ON OPTICAL DAMAGE

A. Introduction and Summary of Results

The experimental work during this reporting period has been devoted to a number of different areas. We have modified and improved the ruby laser so that it operates very reliably (95%) in a single mode. This has been accomplished by the use of a temperature controlled resonant reflector : 2 mm aperture and a dye Q-switch. Extensive energy calibrations have been carried out using different calibrated detectors giving us a more reasonable measure of the uncertainty in our output. Bulk damage threshold measurements have been carried out for a number of ruby and sapphire samples obtained from different sources. Damage at both entrance and exit surfaces has been examined and certain comparisons are made. The differences between the gross characteristics of bulk damage in ruby and sapphire are presented and discussed. The effect on damage threshold of TiO_2 doping has been studied for both ruby and sapphire, and a pronounced lowering of threshold was found (contrary to previously reported results). We have carried out a few experiments in which the damage threshold was measured as a function of optical pumping for both ruby and sapphire. The unexpected results are discussed and further experiments proposed.

B. Experimental Apparatus

The apparatus used in the damage threshold experiments is essentially the same as that described in the previous report (Semi-Annual Report No. 1), and only the modifications will be described. A schematic representation of the apparatus is shown in Fig. 1. The main difference between this apparatus and that shown previously is the use of a dye Q-switch in place of the rotating prism in the laser. We use a solution of cryptocyanine in methanol in a 1 mm pathlength cell the optical transmission of which is 30% at 6943 Å. Another feature not shown in the first apparatus is the MgO diffuser placed after the sample and the associated monitoring detector. The signals from this detector and the one which detects the light reflected from beamsplitter B_2 are integrated and displayed on a Tektronix 555 dual-beam oscilloscope. In addition, beam splitter B_2 has been rotated so that the light is incident much closer

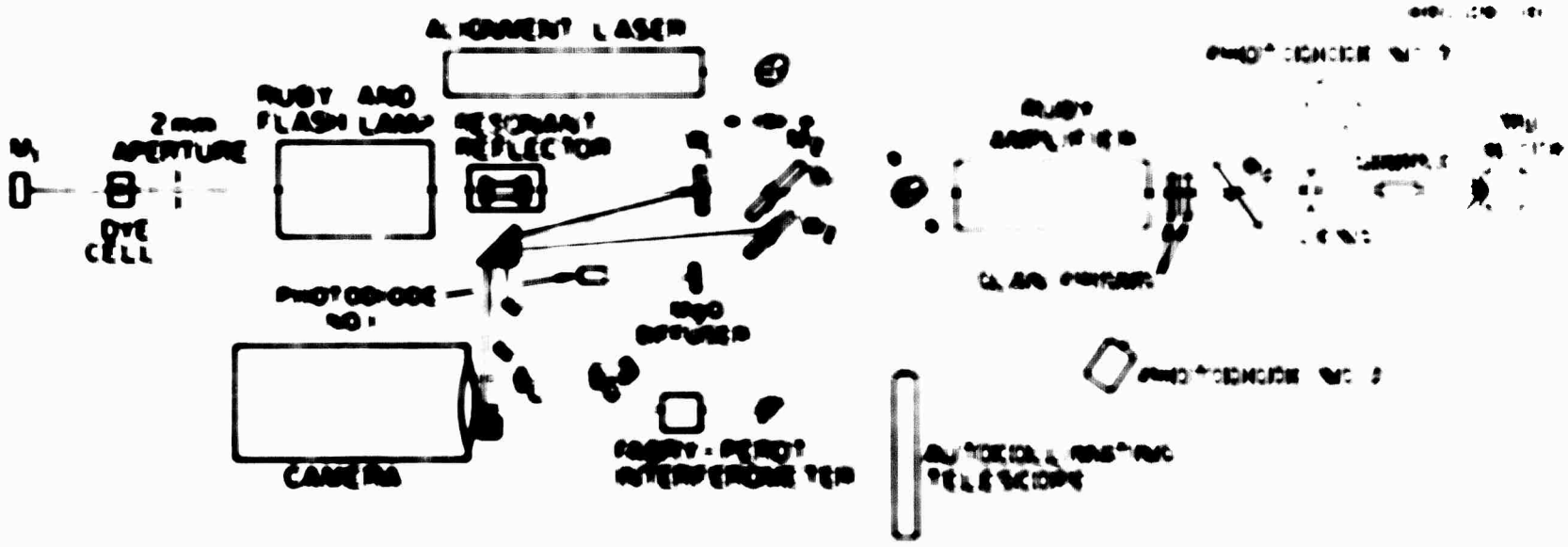

Fig. 1. Schematic representation of experimental apparatus

[illegible] At first we had used a prism to [illegible] the polarization of the beam so as the horizontal plane to maximize the total amount of light removed from the main beam. However, there was a great deal of scatter of the data when the ratio of photodiode No. 2 and No. 3 were compared, even with no change in the beam. The reason for this was not completely clear, but we conjectured that there may have been small changes in the angle of incidence on the beamsplitter #2 due to, perhaps, slight differences in laser alignment from shot to shot. This would result in appreciable changes in the total amount of light reflected into the detector[*]. When the beamsplitter was positioned for smaller angles of incidence where the reflectivity is fairly independent of angle, the problem disappeared. Another feature slightly different from the earlier setup is that photodiode No. 2 looks at the light scattered through a ground glass screen located about 6 in. away. Earlier the screen was much closer [illegible] in.). With this adjustment the signal from the photodiode is much less sensitive to slight changes in position on the ground glass screen which might result from small changes in alignment of the laser.

The two glan prisms shown in Fig. 1 as variable attenuators have not yet been used for that purpose, since we wished to minimize insertion losses in our beam because we often did not have sufficient power to cause damage with the long focal length (40) cm lens. Instead we have varied the pumping line in the amplifier to obtain variations in output power.

One feature of the system as it now exists which leaves something to be desired is the appreciable fluctuation in the power output from the laser. In spite of the fact that the mode properties are very well behaved the power output is apparently very critically dependent on alignment and flash lamp voltage and has been known to change by as much as 50% from shot to shot with no apparent difference in either of the above parameters. Another feature

---

[*]For example, at $\theta = 32°$ a change of 1° gives a 100% change in the reflection coefficient whereas at $\theta = 16°$ the same angular change results in only 1.5% change in reflection coefficient.

[*]All lenses used for focusing the laser into the samples are designed for minimum spherical aberration and antireflection coated. They were obtained from Special Optics.

of the oscillator is that for lower energy pulses the duration of the pulse increases. There the pulse length can vary between about 15 and 25 nsec. We plan to monitor the pump voltage more accurately to see if this improves reproducibility.

We present examples of the data obtained with each shot of the oscillator. Figure 2 shows an example of what we see with our monitoring camera, and Fig. 3 shows a time trace of the laser output taken with photodiode No. 1 and displayed on the Tektronix 519 oscilloscope. Figure 3(a) shows the smooth temporal shape seen about 95% of the time, while Fig. 3(b) shows an extreme example of multimode oscillation. In this case two modes are oscillating with a frequency separation of 750 MHz. This frequency corresponds to the spacing between the end of the ruby and the resonant reflector. The overlapping spectral ranges of the Fabry-Perot interferometer* and the 519 oscilloscope insure that the oscillation of anything other than a single longitudinal mode will be detected.

The amplifier is essentially the same as that described in the previous report except that a modification in the lamp design was made. The reason for this is that the impedance match between the lamp and the pulse-forming network is not optimum. This results in some reflection in the transmission line so that the sample is not pumped as effectively as it could be. The new lamp which has not yet been tested should improve the impedance match and permit more efficient pumping. The maximum gain obtained with the amplifier is about 10 dB. The characteristics of our laser are summarized in Table I.

C. Power and Energy Measurements

Early in this reporting period we discovered that the primary reference used as a power standard in the first measurements (a Korad biplanar photodiode) showed a drastic change in photoresponse. The reason for this is not known. As a result some doubt was cast on the initial power calibration figures. We proceeded to obtain three separate "calibrated" detectors and used them to establish a new standard for photodiode No. 2, our energy monitor. Of these three detectors, two were TRG calibrated thermopiles and the third was a photodiode which had been checked against a number of other calibrated detectors from different sources.

*The Fabry-Perot interferometer has a 3.17 mm spacer giving a free spectral range of 1.58 cm^{-1}. We have measured the resolution to be better than 0.06 cm^{-1} or 1.8 GHz.

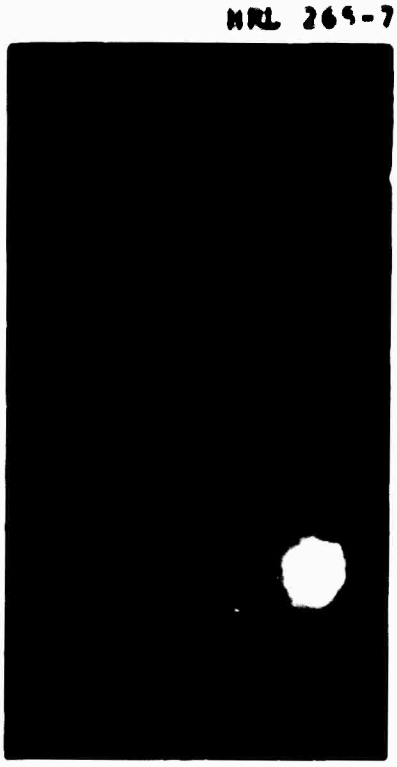

Fig. 2.
Typical photo monitoring Fabry-Perot interferogram, near-field, and far-field beam patterns. The difference in optical density between the two halves of the picture is N.D. 0.6. The free spectral range of the interferometer is 1.6 cm^{-1}.

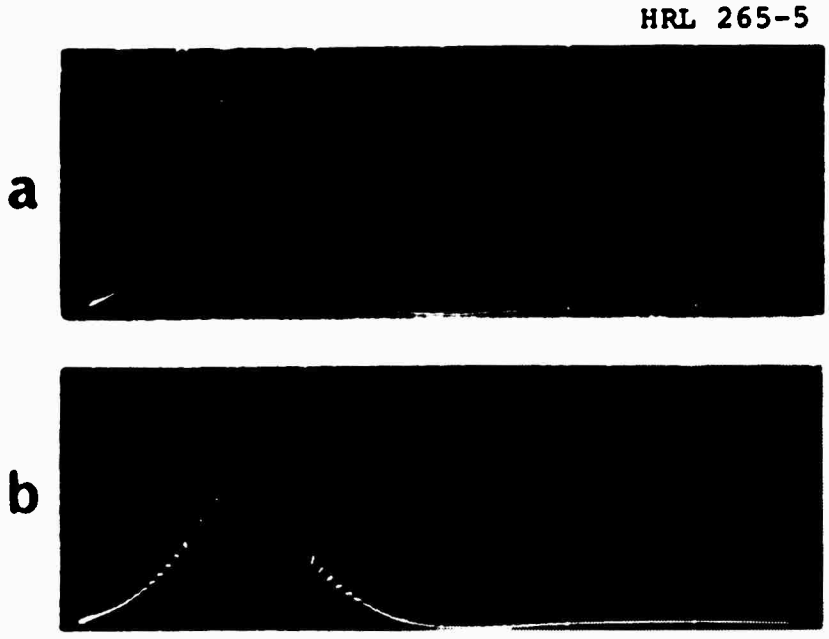

Fig. 3. Tektronix 519 oscilloscope traces of laser output with 20 nsec/division sweep rate. (a) Smooth pulse observed ∿95% of the time.
(b) Modulated pulse (∿750 MHz).

TABLE I

Characteristics of Ruby Laser

Energy Output	12 - 15 mJ
Pulse Length	∿ 20 nsec
Peak Power	0.6 - 0.8 MW
Beam Radius (1/e for E field)	1 mm (±10%)
Beam Divergence	0.6 ± 0.1 mrad (full angle)
Calculated Beam Divergence	0.44 mrad (full angle)

T39

In these experiments the laser and amplifier were fired and signals from the calibrated detectors were compared with that from photodiode No. 2 (Fig. 1). A series of measurements was also taken in which the amplifier was not in place and where both photodiodes No. 1 and No. 2 were compared with the standard detector. In these cases the 519 traces from photodiode No. 1 were integrated, and the integral was compared with the other signals.

The precision of these measurements was very good (∿5%) for each standard detector taken by itself but the three calibrations were not in agreement, the two extremes differing by about 30%. Since our precision is much better than this, we can expect a more accurate power calibration than we obtained at that time. The two thermopiles were sent back to TRG for recalibration. When they return the measurement will be repeated.

D. Gross Characteristics of Damage

We now wish to point out some of the qualitative features of the damage we have observed in ruby and sapphire, and point out the various differences seen in bulk and surface damage.

When we place these samples in the beam we often see some plasma formation at the entrance and exit surfaces; this is shown in Fig. 4(a). In this shot no internal damage was formed, but a small pit was visible at the exit surface.

We wish to emphasize here that exit surface damage is the first to appear in most of our measurements and that the threshold for exit surface damage is about an order of magnitude lower than that for bulk damage. We also notice that the plasma formed at the exit surface is often irregular, sometimes with a pointed appearance in the direction of light propagation; the plasma formed at the entrance surface is more rounded in appearance. Figure 4(b) shows a photograph of another sample in which internal as well as exit surface damage was formed. Here we see a damage track beginning about a third of the way in from the entrance surface. Notice also the flaring out of the beam past the damage track. This blowing up of the beam, discussed briefly in the last report, could be caused by a scattering of light from the damage sites or perhaps by self-focusing and subsequent diffraction. If we assume that the fanning out of the beam is caused by diffraction from a self-focused spot, we can determine roughly the spot size by measuring the angle of the fanned out part of the beam. A crude measurement gives 7×10^{-2} rad for the half-angle, which corresponds to a self-focused spot whose diameter is 6.3 μm. This is not an unrealistically small spot size for self-focusing, and thus the flared out beam could arise from that. On the other hand, we notice that the flared out part of the beam is not very uniform in that the center part has much more light than the outer portions. This would suggest scattering from the damage sites in which a small part of the beam is deflected while most of it continues along the same path.

1. Surface Damage

The difference in the qualitative features of entrance and exit surfaces will be discussed briefly in this section. Figure 5 shows photographs of both the entrance and exit faces of a ruby rod subjected to varying amounts of laser radiation. Note the difference in the kind of damage seen. The exit surface generally shows definite crater formation as was discussed in the last report and illustrated with a number of scanning electron micrographs. The entrance surface on the other hand shows relatively little material lost from the surface.

The influence of entrance surface damage on the apparent threshold for bulk damage has come to our attention during this reporting period. It is possible that one reason for the large fluctuation (see Section I-E) observed in the bulk damage threshold is the generation of damage at the entrance surface and subsequent scattering of light from this damage site (or absorption by the plasma), which

M 7251

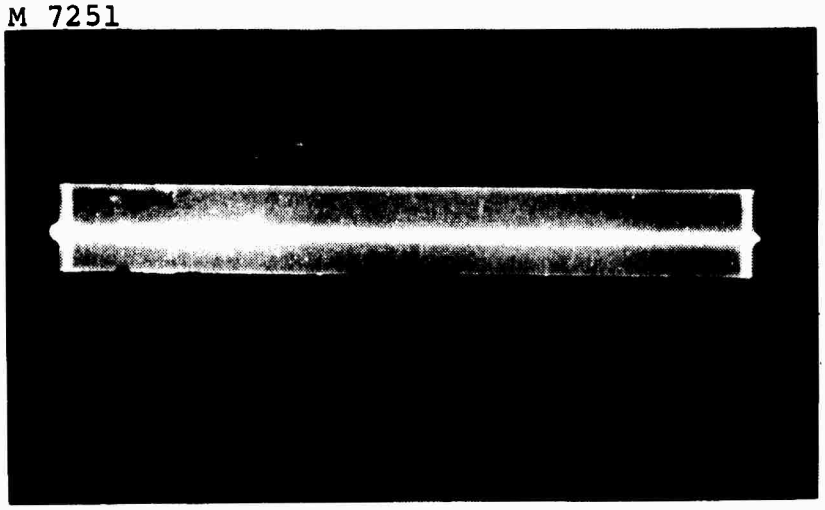

(a) No internal damage.

M 7252

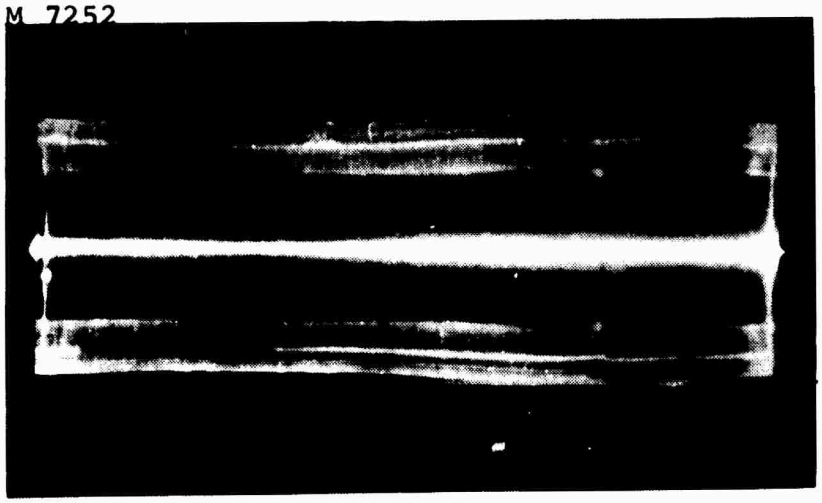

(b) Internal damage plus flaring of beam.

Fig. 4. Photographs of ruby samples while being subjected to laser radiation. Note surface plasma formation. The light is traveling from left to right.

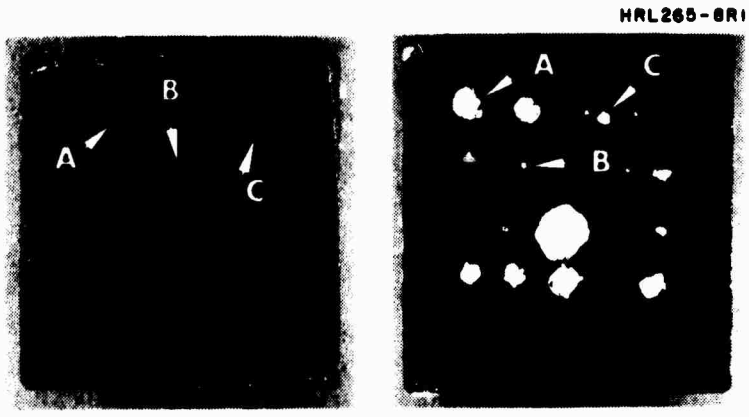

Fig. 5. Exit (right) and entrance (left) surfaces of damaged ruby sample (1/4 in. square) after a number of shots. The regions A,B, and C are relevant to the discussion in the text.

could result in a much lower power density in the interior of the sample than expected. It has been observed that once this entrance surface damage has been formed it is very difficult, if not impossible, to create bulk damage with subsequent shots in the same place. For example, when the same region of the sample is repeatedly irradiated with the laser, each time with increasing power, the bulk damage threshold often cannot be reached; however, the damage on both surfaces generally increases from shot to shot. The problem of surface damage varies considerably from sample to sample and from place to place in a given sample. No substantial difference in this behavior is seen when the surfaces are cleaned with hot nitric acid and rinsed thoroughly with deionized water. (Generally all surfaces are cleaned with ethyl alcohol.)

The photographs in Fig. 5 are presented so that there is a spatial correspondence between the entrance and exit surfaces. As an example of the variation in results for different parts of the sample, let us compare the different regions marked on the photographs. In region A, for example, both entrance and exit damage are observed in a location subjected to several shots from the laser. This region was not damaged internally, even though the power incident on the sample far exceeded that for which internal damage was created in other regions (e.g., region B). Region B is one in which both internal damage and exit surface damage were generated (in this case with one shot), with barely noticeable entrance surface damage. Region C shows a location subjected to a single shot of less than half the total energy as in B. In this case no internal damage was formed but the exit crater is considerably larger than that seen in B. Figure 6 shows entrance and exit surfaces of another sample, where we again see the qualitative features of the different kinds of damage formed. Note the general anticorrelation between the extent of entrance and exit damage as exemplified in Regions A and B. In one case (B) we see exit damage with little or no entrance damage, and in the other we see just the opposite. Next let us compare the entrance and exit surface damage at somewhat higher magnification. Figure 7 shows a magnified view of one of the damage sites seen on the entrance surface of the sample shown in Fig. 6. Here we wish to point out the crazed appearance of the surface. There appears to be a general direction to the crazing on the surface that is the same for all the damage sites examined on that crystal. Other crystals also show this type of linear crazing, but it is not seen on all the samples examined. Figure 8 shows magnified views

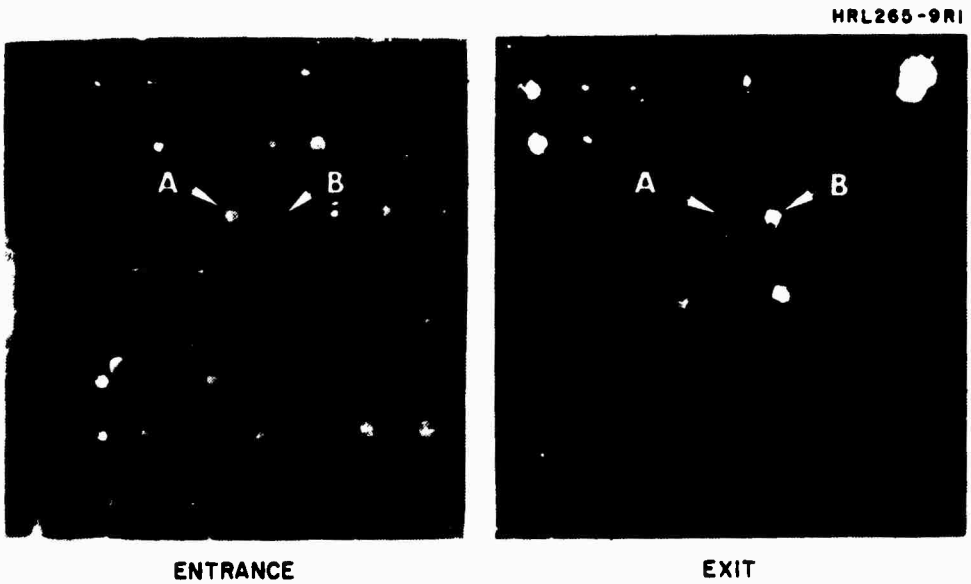

Fig. 6. Exit (right) and entrance (left) surfaces of damaged ruby sample (3/8 in. square). The regions A and B are discussed in the text.

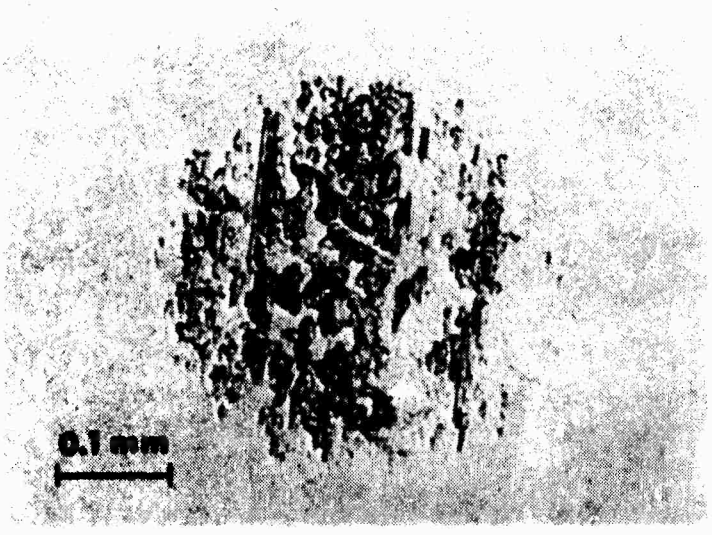

Fig. 7. Magnified view of entrance surface damage such as seen in Figs. 5 and 6.

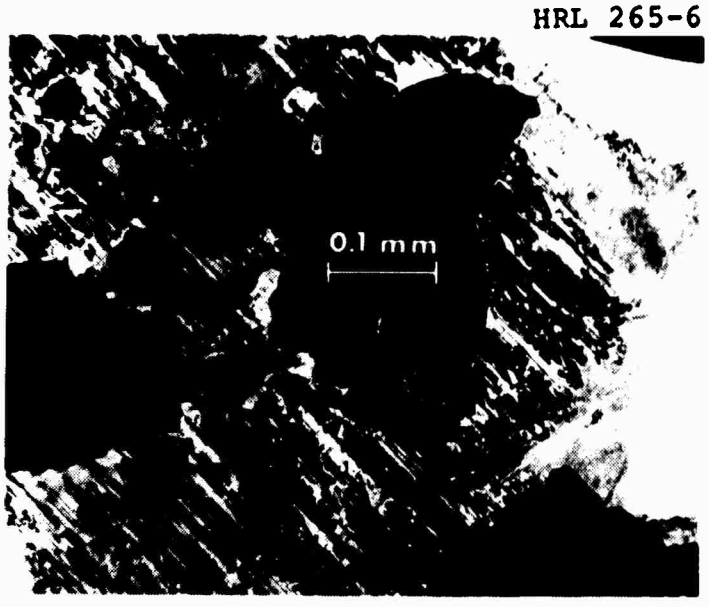

(a) End view.

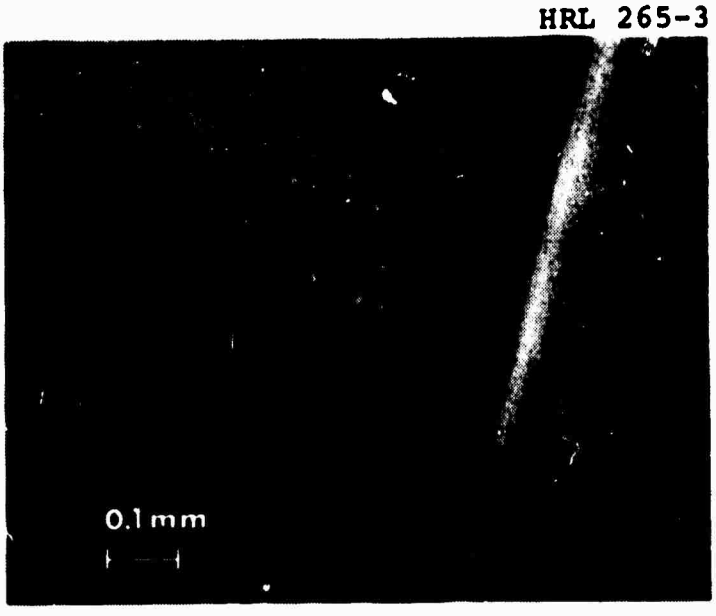

(b) Side view.

Fig. 8. Photomicrographs of exit surface damage pits and crazing.

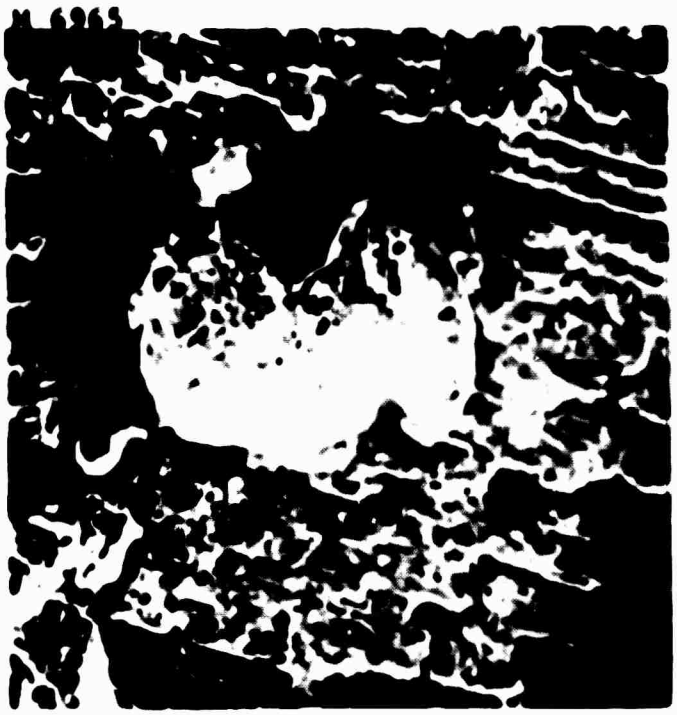

Fig. 9. Scanning electron micrograph of exit surface damage in ruby showing crazed region and surface pitting. Marker length is 15 μm.

of exit surface damage. In the last report we presented a number of pictures of exit surface damage taken with a scanning electron microscope. We reproduce one of those at this time in Fig. 9 for the purposes of the present discussion. Note that the exit surface damage consists of pitting or crater formation, as well as the crazing similar to that seen on the entrance surface.

3. Bulk Damage

During these studies we have noticed a difference between the qualitative features of the bulk damage in ruby, compared with sapphire. This is illustrated in Figs. 10 and 11. In Fig. 10 we see some typical damage tracks seen in a ruby sample. These tracks appear to be a series of bubbles or small fractured regions of variable spacing; they are more densely packed at the beginning of the track and spread out toward the end, so that in some cases there is an appreciable gap between damage sites in a given damage track. The beginning of the track generally shows a more densely damaged region that is usually much wider than the rest of the track. In contrast, the bulk damage in sapphire appears to be qualitatively different. In Fig. 11 we see an example of typical damage tracks observed in sapphire. These are generally more continuous (fewer interruptions) than those seen in ruby, and often contain a "hollow" core with fractured regions at the periphery (see a in Fig. 11).

In this particular sample there were a few irregular tracks such as that shown in b of Fig. 11). It is curious to note that these tracks occurred when there was appreciable temporal modulation on the laser pulse. When these measurements were made there was an unusually high percentage of modulated shots. It was noted that the irregular damage occurred only on those shots when the pulse was modulated (about six times). We offer no interpretation of this observation, but merely point it out as a curious occurrence.

This section may be summarized with the following statements concerning the qualitative features of the damage in ruby and sapphire.

There are three distinctly different types of damage: bulk, entrance surface, and exit surface damage. The surface damage appears to be similar in both ruby and sapphire while the bulk damage differs as described above.

HRL 265-2

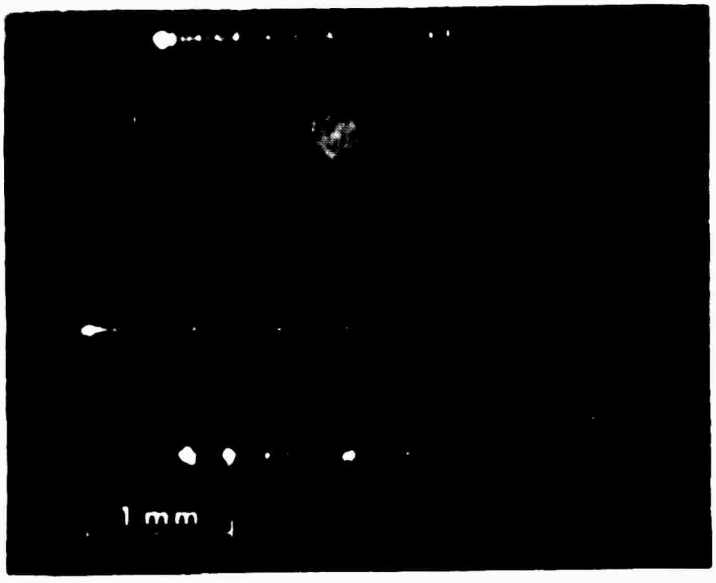

Fig. 10. Photomicrograph of damage tracks in ruby (see text for discussion).

HRL 265-1R1

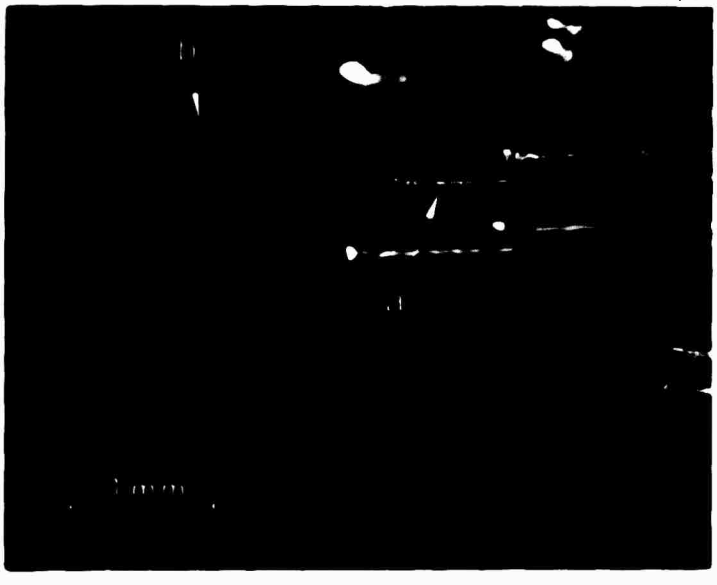

Fig. 11. Photomicrograph of damage tracks in sapphire (see text for discussion).

Entrance and exit surface damage are similar in two respects and differ in a third. They are similar in that plasmas occur at both surfaces and both show some crazing at the damage site. They differ in that a fracture crater occurs on the exit and not on the entrance surface. We suspect that the crazing is connected with and perhaps caused by the plasma that is seen at both surfaces, whereas the crater, which is unique to the exit surface, is generated by a phenomenon that takes place in the bulk of the material and manifests itself at the surface.

The threshold for exit surface damage is about an order of magnitude lower than that for bulk damage. It is more difficult to make a definitive statement concerning the relative thresholds for entrance surface damage and internal damage. The ease of plasma formation at the entrance appears to be a function of undetermined surface parameters, the most likely of which are adsorbed substances and surface finish.* Therefore, the state of the entrance surface definitely determines what occurs inside the crystal and at the exit surface. In the extreme case all of the light could be dissipated in the entrance plasma.

Finally, let us assume that a hypothetical sample is subjected to a series of shots with increasing energy, each time striking a different spot, and assume that the power density is uniform over the length of the sample. We will first observe exit surface damage at some threshold. As the energy is increased, the extent of the exit surface damage will increase to give a larger crater than on the previous shot. At an order of magnitude higher input we reach the threshold for bulk damage, at which point a short damage track will appear; at the same time, we will probably observe a decrease in the size of the exit pit relative to what it was just below bulk damage threshold. As we increase the energy further we will generally observe more extensive internal damage and perhaps begin to see some entrance surface damage, depending on the condition of the entrance surface. At still higher incident energy the extent of entrance surface damage (or absorption by the plasma) can be so great that it precludes the formation of bulk damage simply because not enough light gets inside to cause damage.

*It is definitely known that a substantial plasma will form on a dirty entrance surface. In addition, in our limited observations it appears that those crystals with more surface scratches are more easily damaged at the entrance surface.

E. Damage Threshold Experiments

In this section we present the results of damage threshold experiments for internal damage in a number of different materials from various sources. In all the cases presented the data represent a large number of shots for a given sample. There was a large amount of scatter in the data, as mentioned earlier; we believe this results in part from the varying amount of plasma formed at the entrance surface. It is also reasonable to believe that there is an intrinsic variation in damage threshold from place to place in the same sample. As a result, there is a range of incident energies over which one may or may not see internal damage, depending on the particular location in the crystal. For example, at a particular location in the sample no damage is seen at a given incident energy, while extensive damage may be seen in another part of the sample for a lower energy in another shot. The data presented in Fig. 12 reflect this fact. The dashed line corresponds to a range of power densities where damage was not observed at some locations in a given sample and is terminated on the high end by the highest power for which internal damage was not created. The solid line corresponds to input energies where damage was observed at some locations in the same sample and is terminated on the low end by the smallest input energy for which damage was observed. For example, let us examine the data presented for Cz Ruby L104 in Fig. 12. The dashed line shows that certain regions of the sample were subjected to power densities up to 7.1 GW/cm^2 without damage. The solid line shows that damage was observed in some other parts of the sample at input power densities as low as 6.3 GW/cm^2. Thus, the amount of overlap gives a measure of the definability of damage threshold for a given sample.

The power densities in Fig. 12 are calculated power densities at the beam waist. Mode propagation equations described previously were used to compute beam radius and divergence at various locations. The energy incident on the focusing lens first is measured by photodiode No. 2 (Fig. 1). This is converted to power by dividing by the appropriate pulse width (FWHM) as determined by the Tektronix 519 oscillograms. The power density at the lens is computed by dividing this power by the area of the beam at the lens. This gives a spatial average for the power density or energy density. The energy density at the peak of the gaussian

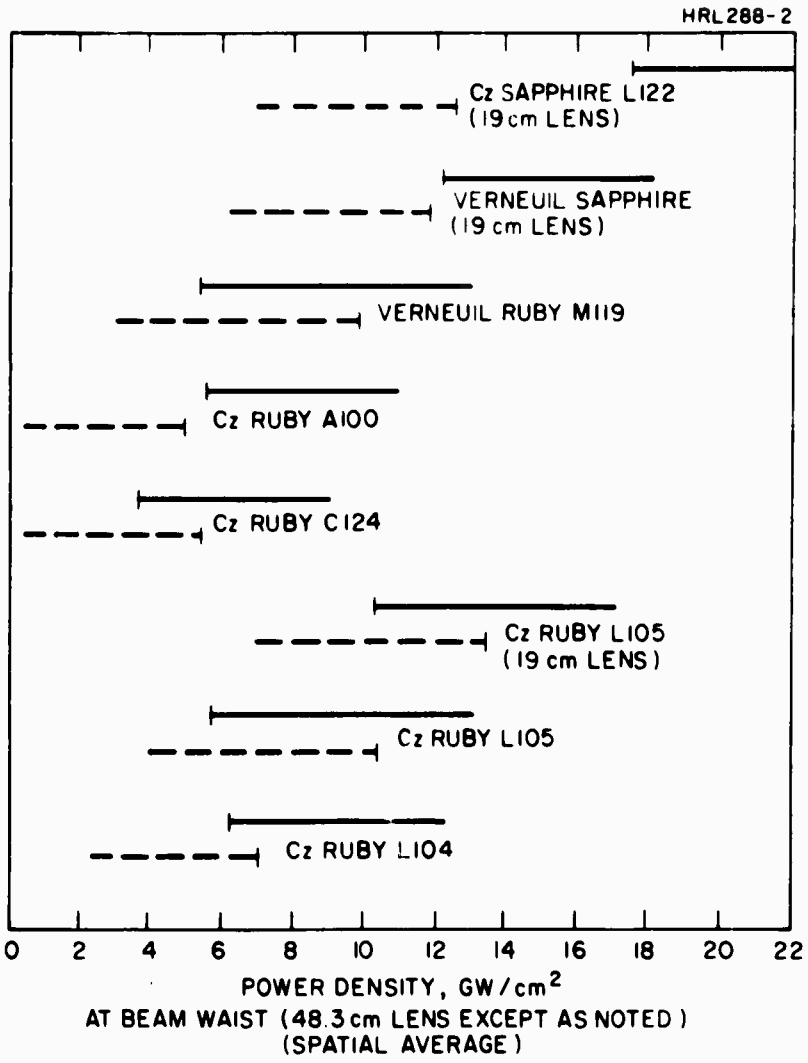

Fig. 12.
Bulk damage thresholds for a number of ruby and sapphire samples. The power density and energy density scales are spatial averages. The power and energy densities at the peak of the gaussian distribution are twice the spatial averages (see text). The dashed line corresponds to power where damage was not observed; the solid line to powers where damage was observed for a number of shots in different regions of the same sample.
Sample sources:
A100 - Airtron
L104, L105, L122 - Union Carbide
C124 - Crystal Optics
M118, M119 - Meller.

distribution is twice the spatial average.* The power density at the focus of the lens is obtained by computing the beam size at the focus.

We wish to emphasize that these power and energy densities are based on the following assumptions: (1) The spatial profile of the output is gaussian with a 1 mm radius (1/e radius for the electric field.) (2) the spreading of the beam is by diffraction only, and the beam suffers no distortion, focusing, or defocusing in passing through the ruby amplifier. (3) The diffraction limited spot size is reached at the focal plane of the focusing lens. The degree to which these assumptions reflect the reality of the physical situation can only be estimated at present, pending further measurements. Measurements of the near field spot size at the oscillator output mirror give a 1 mm radius for the 1/e points of the electric field (assuming a gaussian distribution). This was done both by photographing a pair of spots on a ground glass screen with a known attenuation difference and by measuring the sizes of burn patterns on Polaroid film, with the relative energies of successive shots known. The measurements by both techniques agree to better than 15%. Measurements of the far-field divergence of the oscillator give values that are higher than that expected for a gaussian, although the measurements are not highly accurate. We obtain 0.6 ± 0.1 mrad (full angle) from relative spot size measurements in the focal plane of the 1 m focal length camera.† The calculated beam divergence gives 0.44 mrad ($\theta \simeq (2\lambda)/(\pi\omega_o)$; full angle);

*The gaussian beam radius ω is defined as the radius for which the electric field reaches 1/e of its peak value. This is the radius for which the intensity or the energy density reaches $1/e^2$ of its peak value. If we define a beam area $A = \pi\omega^2$ and divide this into the total energy E_{tot}, we have a kind of average energy density. It is easy to show that the energy density at the peak of the gaussian distribution is $2E_{tot}/\pi\omega^2$. In most of the reports in the literature the power densities or energy densities refer to a kind of average. That is, the total energy is divided by the "beam size" determined by some means or other. This method is convenient when the spatial power distribution is not known.

†It is easy to show that the 1/e diameter for the intensity is $D_I = \sqrt{d_1^2 - d_2^2}/\sqrt{\ell n\ \alpha}$, where d_1 and d_2 are the measured spot diameters and α is the ratio of the intensities (for density 0.6, $\alpha = 4$). The 1/e diameter for the field is $D_E = \sqrt{2}\ D_I$.

this is appreciably lower than that observed but is almost within the uncertainty of measurement. Even though we are well below the saturation flux for the amplifier ($4 J/cm^2$ compared with 15 J/cm^2), the uncertainty in the effect on the beam properties of the amplifier is probably the largest and most difficult to estimate. Characterization of the beam after passing through the amplifier will be carried out soon.

F. Dependence of Damage Threshold on Added TiO_2

Recent work of Nath and Walda[1] reported a striking increase (40x) in the damage threshold in sapphire when small amounts (20 to 100 ppm) of TiO_2 were added. We decided to check these results and extend them to ruby as well. We purchased Verneuil ruby and sapphire samples from the same source used by the above workers (Djeva in Switzerland via Adolf Meller Co.), both undoped and doped with nominally 30 ppm TiO_2. The thresholds for internal damage were measured, and the results were found to be essentially opposite those reported previously. Table II shows the results of these measurements. The numbers in the table are given in pairs. As discussed in connection with the data in Fig. 12, the numbers reflect the variation of threshold from place to place in the sample. Of the two numbers quoted, that on the left is the highest value for which damage was not observed in the sample, and that on the right is the lowest value for which damage was found in the same sample. We see from Table II that the thresholds for the titanium doped samples are at least an order of magnitude lower* than those for undoped samples. The reason for this discrepancy with the results of Nath and Walda is not known. In addition, contrary to the results of Nath and Walda, we found that the ultraviolet absorption edge for the TiO_2 doped samples occurred at a shorter wavelength than that for the undoped sapphire (2600 versus 2300 Å). This is shown in Fig. 13.

---

[1] G. Nath and G. Walda, "Strong Radiation of Laser Produced Damage in Sapphire and Ruby by Doping with TiO_2," Z. Naturforsch. 23a, 624-625 (1968).

*These titanium doped samples are examples of ruby and sapphire for which the bulk damage threshold is so low that surface damage does not form.

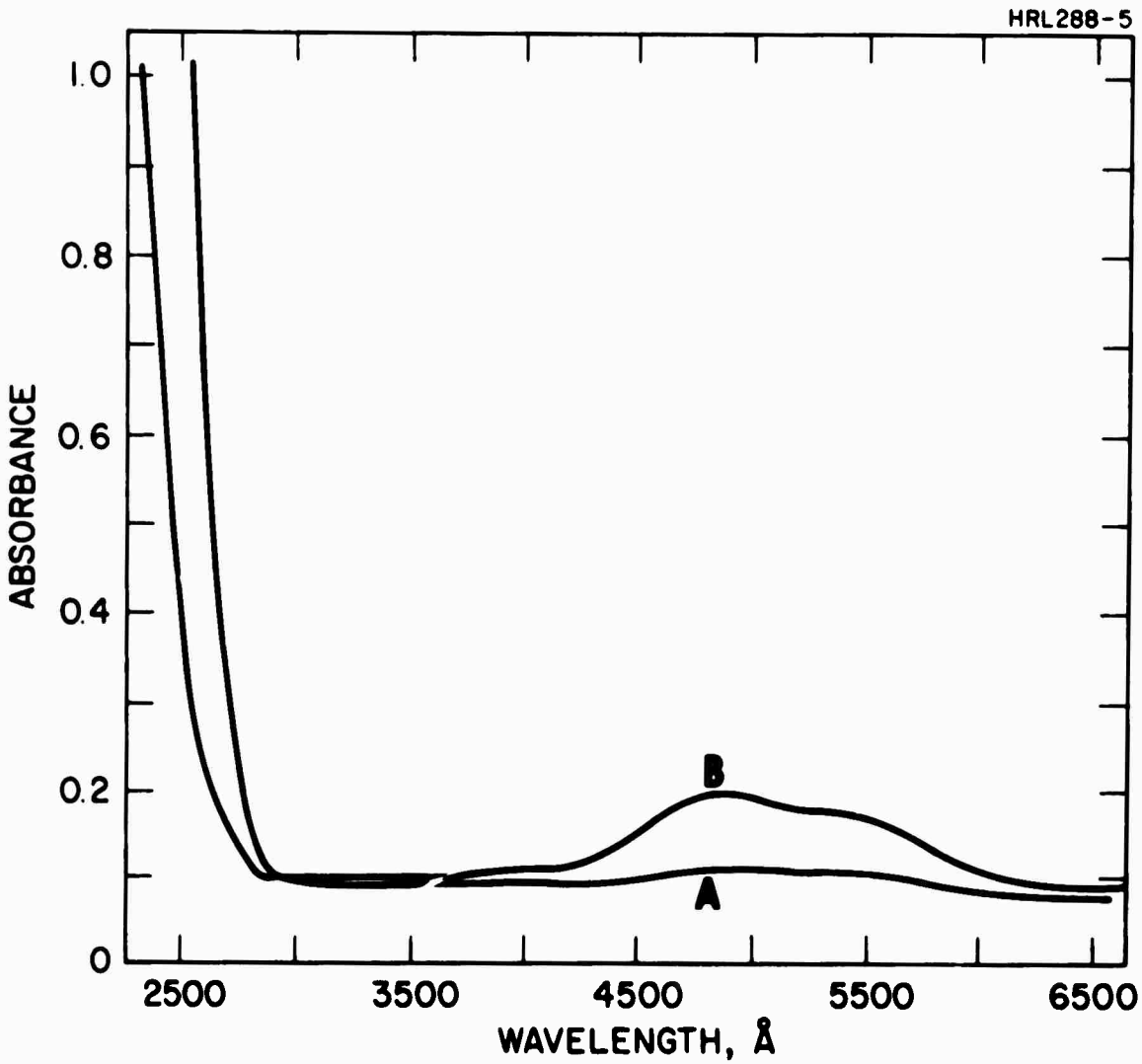

Fig. 13. Absorption spectra of Verneuil sapphire whose thresholds are reported in Table II. (a) Undoped. (b) 30 ppm TiO_2. These spectra were taken with a Cary 14 spectrophotometer using air as a reference.

TABLE II

Effect of TiO_2 Doping on Damage Threshold

	Power Density for Internal Damage, GW/cm^2	
	Without TiO_2	With 30 ppm TiO_2
Verneuil Ruby	5.4, 9.9	0.94, 0.70
Verneuil Sapphire	12.1, 9.4	0.36, 0.52

T40

Because of these discrepancies it is reasonable to suspect that we may in fact have different material from that studied by Nath and Walda. The future course of this work is at present uncertain.

G. Optical Pumping Experiments

During this reporting period we have carried out a few experiments in which we optically pumped the samples while subjecting them to the laser radiation. Figure 14 shows the apparatus used for optically pumping. It was designed so that the sample could be examined closely between shots without the need for removal from the apparatus. The experiments were carried out on two ruby samples and one sapphire sample.

The samples were pumped with a power supply similar to that used for pumping the amplifier flash lamp. In these experiments we pumped at two different levels (1200 J and 3700 J) into the flash lamp (model FX60 by E.G.&G.). As in the previous experiments we fired a number of shots (generally 10 to 20) at each pumping level for a given sample.

The results of the threshold versus pumping experiments are shown in Fig. 15. Here the results are depicted in a manner similar to that of Fig. 12, where the dashed line refers to the powers where no damage was seen in some parts of the crystal and the solid line to powers where damage was seen in other parts. The scatter in the data is relatively high, but nevertheless we can confidently say that there is no appreciable lowering of the threshold with optical pumping and, if anything, there may be a slight increase.

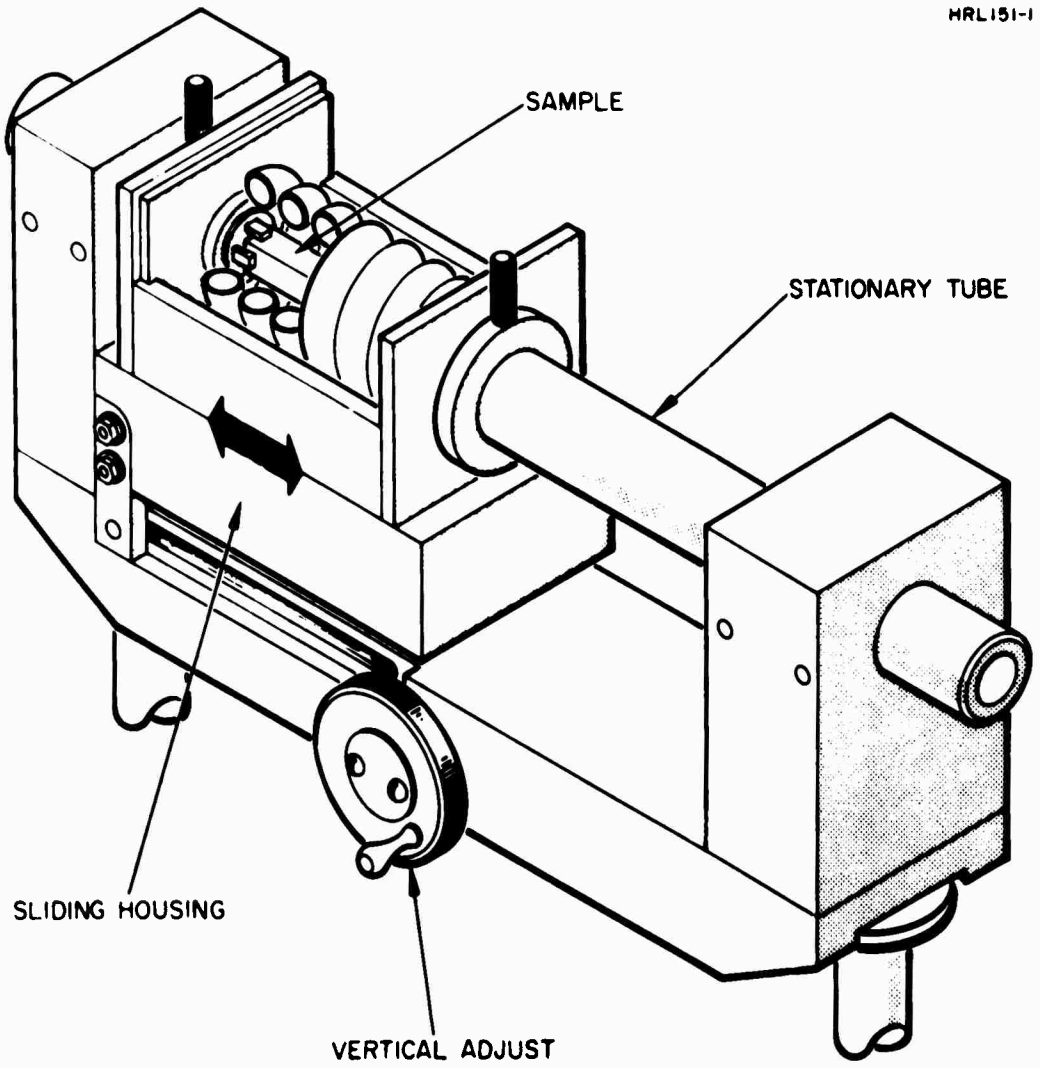

Fig. 14. Apparatus used for optical pumping experiments.

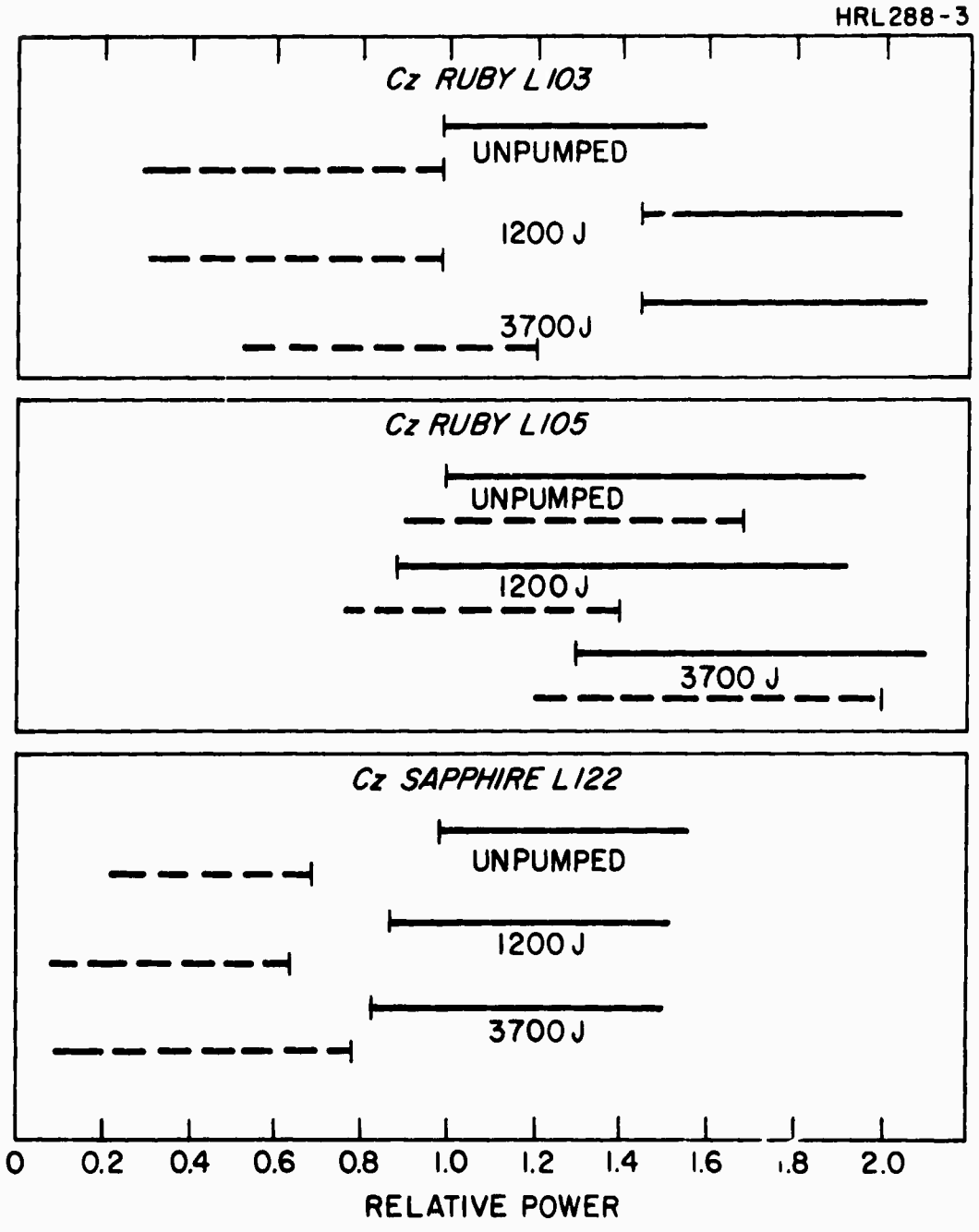

Fig. 15. Relative bulk damage threshold as a function of optical pumping for different samples. The threshold are normalized to unity for each sample (unpumped). Dashed line – no damage; solid line – damage.

One reason for the scatter in this case is the use of a shorter focal length lens than has been generally used (19 cm compared with 48 cm). We used this lens because the output from our system was somewhat lower than previously and we were not quite able to reach damage threshold with the long focal length lens. A more extensive plasma was formed at the entrance surface at times when the 19 cm lens was used, and an appreciable fraction of the light undoubtedly was absorbed by the plasma. The experiments will be repeated with the sample in a different position so that this will not occur as readily.

We observed another interesting phenomenon in these pumping experiments related to the location of the damage in the crystal as a function of pumping. In ruby that is not externally pumped, we see damage tracks whose beginning is usually uniquely located in the sample. That is, for a number of shots at different powers we find that the damage tracks begin at roughly the same distance from the entrance surface. The length of a given track generally will be longer for higher power.

When the ruby samples are optically pumped, we see damage tracks that begin at an appreciably different location "downstream" from the tracks for the unpumped sample. Harder pumping shifts the tracks even more. This phenomenon is reversible; results for a sequence of nonpumping, pumping, nonpumping, pumping are reproducible.

The results of these experiments are shown in Fig. 16, where the location of the beginning of the damage track is plotted as a function of energy discharged into the flash lamp. The lengths of the bars on the plot reflect the variation in position from shot to shot of the beginning of the damage track.

This effect of apparent defocusing of the light cannot be explained as a sort of thermal focusing due to the optical pumping; it is much too large for that. For example, if we were to assume that the ruby has somehow become a negative lens, we might ask what the effective focal length would be. Taking into account the distance of the entrance surface of the ruby from the lens and assuming that the shift in the location of the damage track corresponds to a shift in focus, we compute that the ruby would have to act as a negative lens of $\sim$20 cm focal length, which corresponds to a radius of curvature of the end of the rod of $\sim$7 cm.

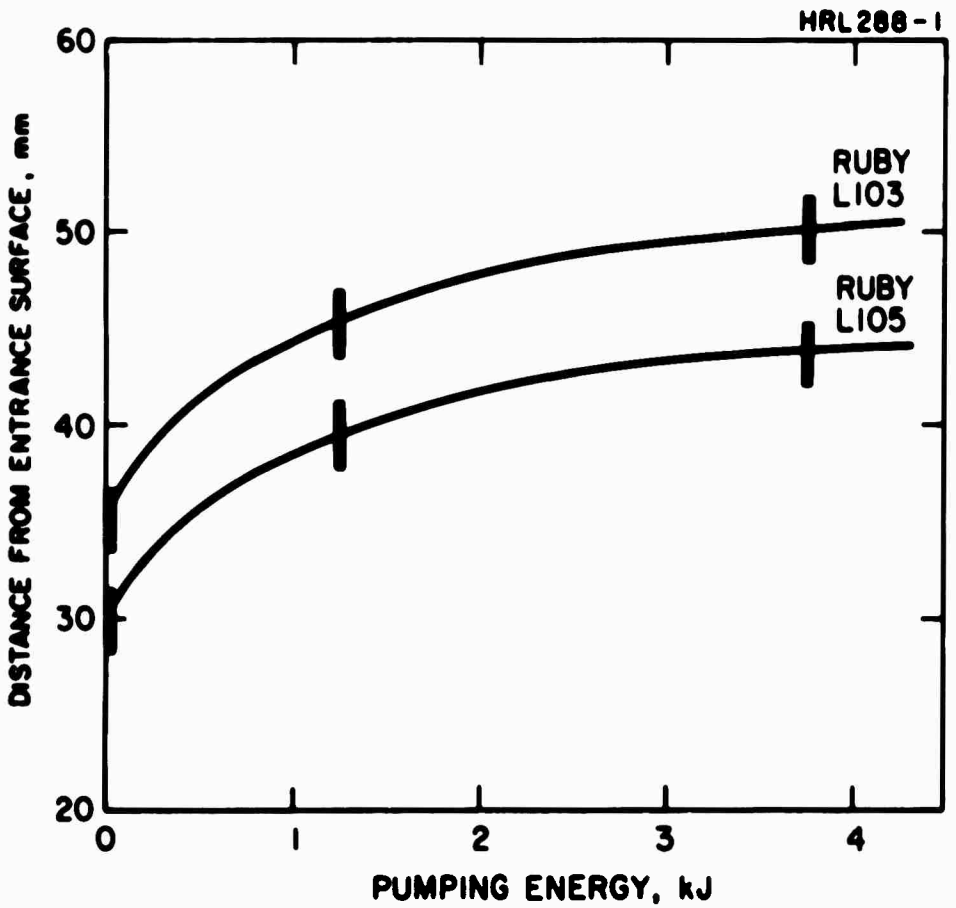

Fig. 16. Location of beginning of damage tracks from entrance surface versus optical pumping energy for ruby samples. L103 - 0.03% Cr^{+3}, L105 - 0.05% Cr^{+3}.

Alternatively, we can compute the apparent change in refractive index with pumping to account for the shift in the position of the damage track. The relative shift in the distance from the entrance surface to the focus is directly proportional to the relative change in refractive index. This then corresponds to an apparent index change of 40 to 50%, a very large effect!

It is difficult to account for this effect by postulating any change in the linear refractive index. A decrease in nonlinear index that somehow depends on the degree of optical pumping is a possible explanation, but this should result in a higher damage threshold for pumping than for nonpumping. This may be the case, but there is too much scatter in the data to confirm this (Fig. 15). We also mentioned that in the pumping experiments there was a substantial amount of plasma formation at the entrance surface. It is conceivable that optical pumping of the surface plasma could lead to some defocusing effect. It is clear that more experiments in this area are needed, especially with regard to the relative damage thresholds.

A correlation for sapphire similar to those seen for ruby in Fig. 16 does not exist. The location of the beginning of the damage tracks in unpumped sapphire varies over a much wider range, depending on the incident energy from the laser, and any effect of optical pumping is obscured by this variation.

When the incident laser power is close to threshold the damage is found farther "downstream"; as the incident energy increases, the location of the beginning of the track moves "upstream" toward the source. This is illustrated in Fig. 17, where we plot the distance of the beginning of the damage tracks from the entrance surface versus laser power incident on the focusing lens.

H. Plans for Next Period

One of the first tasks to carry out will be the measurement of the beam characteristics after the amplifier. Dependence of damage threshold on the size of the focal spot will be studied, and the optical pumping experiments will be repeated in an attempt to obtain better reproducibility in the data. The evolution in time of the damage track will be studied using an image converter camera.

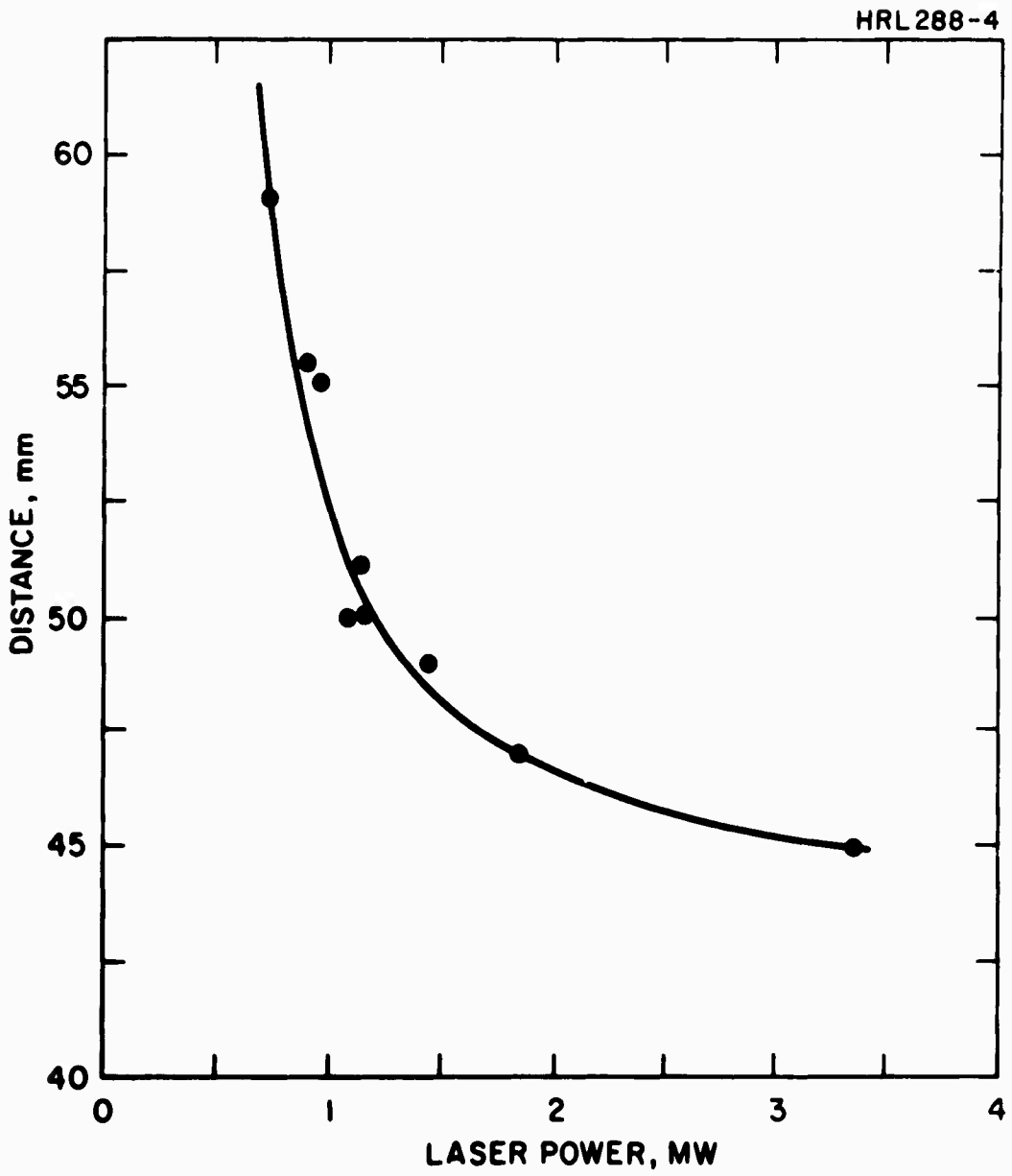

Fig. 17. Location of beginning of damage tracks from entrance surface versus laser power incident on 19 cm lens for Cz sapphire sample L122.

BLANK PAGE

II. THEORETICAL STUDIES ON OPTICAL DAMAGE

A. Introduction

In the theoretical studies conducted for this project we have first established a broad outline or "scenario" of optical damage as it is caused in the best quality ruby and sapphire by laser pulses of order 20 nsec duration and shorter. This general examination then led us to a concentrated study of a previously unexplored class of mechanisms which we thought might play a central role in the breakdown of sapphire and ruby. These mechanisms involved the ability of a relatively low-density ($\sim 10^{16}$ cm^{-3}) of cold photoexcited conduction electrons (1) to transfer energy rapidly and efficiently from the optical beam to the lattice and (2) to accelerate the excitation of even more conduction electrons, thus aiding further in the energy transfer of (1). In subsection B we review the general damage picture as we see it, and then in subsection C the results of our studies of photoelectron dynamics in strong optical fields are presented. For details pertinent to these sections, the reader will be referred to a paper which is reproduced here as an Appendix.

B. A Proposed General Outline of the Process of Optical Damage in Sapphire and Ruby

We have found it useful to view in five stages the over-all damage process in ruby or sapphire (often referred to as "the crystal"). These stages are as follows:

(1) Before actual physical rupture of the lattice occurs, a certain spatial and temporal distribution of optical fields that is able to initiate the damage process is reached or exceeded in the crystal. A comprehensive description of the threshold beam conditions for short pulses is far from being complete, being dependent on the outcome of researches on all the phases of the damage process. Roughly speaking, it is believed that if the beam can deposit from 10^2 to 10^3 J/cm^3 in a small region of the crystal in less time than it takes heat to diffuse out of the region, then a rupturing shock wave will develop. As a working rule of thumb, a pulse of duration 10^{-8} to 10^{-10} sec and of order 10^{-2} cm in diameter cannot exceed several times 10^{10} W/cm^2 peak intensity without initiating damage in ruby or sapphire. However, several remarks are in order.

First, the visual appearance of damage tracks suggests that self-focusing of the optical beam is instrumental in increasing the beam intensities into the damaging regime. This is not definitely established and is under investigation in this project and elsewhere. However, if self-focusing is aiding in the initiation of damage, then the above numbers have grown out of some probably incorrect interpretations of data and may require modification. To better establish the degree of self-focusing, a definitive measurement of the "fast-responding" part of the nonlinear index of sapphire and ruby would be helpful. Early in this project, we examined the possibility that transient electrostriction could produce self-focusing at observed damage power thresholds and found it to be extremely remote. Whether or not self-focusing is occurring from other mechanisms we view the subsequent stages of damage roughly as follows.

(2) The intense optical beam next promotes a number density of order 10^{16} electrons/cc from impurity levels into the conduction band. This can happen by the direct or "linear" photoexcitation process observed by Hochuli (Ref. [5] of the Appendix) at low optical intensities ($\sim$5 W/cm^2). More likely, this excitation is produced by complex multistage, or even "bootstrap" avalanche, processes that resulted in the highly nonlinear photoconductivity observed by Belikova, et al. (Refs. [7,8] of Appendix), at high optical intensities ($\sim 10^{10}$ W/cm^2). The studies of some new processes of the latter kind made under this project are discussed in subsection C.

(3) The strong optical field seen by electrons reaching the conduction band imparts to them some added random motion (heating) and some coherent oscillatory motion. Previous workers have concentrated on the heating effect (Refs. [1-4] of Appendix), supposing that the electrons might gain enough random energy to ionize the lattice, promoting other electrons across the band gap ($\sim$ 8 eV) in an avalanche process. We have examined this possibility in detail starting, as did previous workers, from Fröhlich's well-known model for electron-lattice interactions. We found to be negligibly small the probability of an electron's gaining even one eV of random energy at nominal damage intensities ($\sim 10^{10}$ W/cm^2). However, when we examined the effects of the low-energy coherent motion ($\sim 10^{-3}$ eV) of a "cold" electron in the intense field superposed on the small thermal motions (appropriate to a temperature not much above the ambient lattice temperature), we found a potentially damaging situation. These oscillating electrons spontaneously

radiate longitudinal optical (LO) phonons at a significant rate, much as an electromagnetic antenna radiates photons. (We also calculated the rate of stimulated emission of phonons by the oscillating electrons but found this to be negligible.) Our efforts in assessing this phonon radiation rate are described in subsection C.

(4) The LO phonons radiated by the conduction electrons have a nearly vanishing group velocity and do not carry their energy out of the region of the beam rapidly. Although direct measurements of the lifetimes of the most important phonons (which do not have a small wavevector) are unavailable, we believe that they decay rapidly into acoustic phonons in a time short compared to laser pulse lengths, in essence depositing a certain thermal energy very close to the electrons that radiated them. This means that there is an equivalent heat source formed in the irradiated parts of the crystal.

(5) In the final stage of damage, the large random acoustic (heat) energy generated from the LO phonons forms shock waves which then rupture the crystal, generally some time after the optical pulse has passed. It is not beyond the theory of shock waves in solids to estimate the strains developed as they propagate away from the heated region. However, it would be a formidable computing task and we have not attempted it. Other efforts in the project have been concentrated as outlined in the following section. Before discussing these efforts, however, we might make a few critical remarks about the above review of damage.

There are various potentially damaging processes which lie outside the foregoing outlines. We have examined all of those known to us and have found them to be probably less important than those outlined, or at best only occurring in a final holocaust when they are not needed, if indeed they would still be identifiable. Among the most prominent of these are stimulated Brillouin, Rayleigh, and Raman scattering. In the first two instances, we have investigated the degree of stimulation of density waves for purely electrostrictive and for absorptive (thermal) coupling. It seems very unlikely from existing electrostrictive data that significant stimulated Brillouin waves would develop. Significant gain from absorptive coupling exists if some mechanism (such as our conduction electron mechanism) can produce optical absorption of order one cm^{-1}. But at this level of absorption, damage from other effects of the heating will certainly obscure any stimulated effects.

Raman scattering cross sections are not well known, but there has never been observed at damage the distinctive strong Stokes and anti-Stokes sidebands that accompany stimulated Raman scattering.

C. The Role of Photoelectrons in Crystal Damage

In this project we have examined two of the many questions surrounding the roles of photoelectrons in the various stages of the damage process which we outlined in the preceding section. First, we have studied the rate at which a single conduction electron transfers energy from the optical field to the LO phonons. Second, we have estimated how the presence of conduction electrons at densities of the order of 10^{16}/cc affects the rates at which electrons initially bound to impurities (dislocations, foreign ions, etc.) make transitions to higher energy impurity levels, both bound and unbound.

The first question has been answered with the most surety. Fortunately, sapphire and ruby are polar crystals, and in polar crystals the interactions of cold electrons with the LO phonons dominate their interactions with other phonons; and a particularly simple model of this interaction derived first by Fröhlich (Ref. [10] of Appendix) has proven to give remarkably accurate predictions of mobilities, effective masses, and even cyclotron level shifts in a wide variety of materials. The only parameters in this model are the static and optical dielectric constants, the LO phonon frequency (or its average), and the effective band mass of the conduction electron. Unfortunately, the last is not known for sapphire, but experience with other ionic, high band gap materials indicates it is easily within order of magnitude of the free electron mass. More fortunately, the rates we seek do not depend too strongly on the effective band mass, typically varying as its square root. A further complication is that the electron-phonon interactions in sapphire and ruby cannot be treated by quantum perturbation theory. The dimensionless perturbation expansion parameter α defined by Fröhlich is roughly three in this case, and only for $\alpha \ll 1$ is perturbation theory accurate. The author, with others, has previously developed a method for treating such cases of "intermediate coupling" (Ref. [6] of Appendix). This method is based on a minimum-variational principle. Long experience with a certain two-parameter variational function has indicated that, used in computing

the electron response in the manner prescribed in Ref. [6] of the Appendix, this function will yield an optical absorption rate for a conduction electron accurate to within ~10%. The uncertainty in the band mass contributes much more uncertainty in our final results, so refinements of the variation function, or in other approximations in its use, are not warranted. The numerical details of this calculation of the optical response, and from it the phonon radiation rate, of an electron in sapphire or ruby are given in Section 4 of the paper reproduced as the Appendix.

The second question studied in this project sought to determine whether the presence of $\sim 10^{16}$ conduction electrons/cc could significantly affect the rate in which impurity electrons made up their ladder of levels and hence contribute to the very nonlinear behavior of the dc photoconductivity observed by Belikova, et al. (Refs. [7,8] of Appendix), in what are probably the only high-intensity experiments reported to date which avoided many spurious effects of surface conductivity. The impurity level structure of sapphire and ruby is seen to be very weak but very complex from existing infrared absorption and luminescence data. Unfortunately, the densities of impurities of different types are completely unknown as is the structure of any given type. One can make crude estimates, however, with various physical models, of the transition matrix elements required in a simple Born approximation or dipole approximation treatment of optical field-electron-impurity interactions. Using what we felt were conservative guesses, we found that the impurity transition rates could be affected in an important way by the conduction electrons. This is especially true for the majority of bound-bound transitions normally not resonant with the optical beam, for these transitions become allowed when the conduction electrons can carry away the excess transition energy. Optical cross sections for such electron-enhanced transitions are found to be of the order of 10^{-22} cm^2. Therefore, impurity densities of order 10^{19} cm^{-3} might bring these processes into contention, if not dominance, over direct photoexcitation. The details of these calculations are given in Section 5 of the Appendix.

Many other questions surrounding the role of photoelectrons in damage have been or are currently under study (see, for example, the Appendix). However, without much more reliable and wider range of experimental data on the impurity level structure and conduction band characteristics in optical materials of interest, definitive answers cannot

be found for what causes damage, how to prevent it, and how to detect damage-prone crystals before use. Fortunately, laser sources provide an unprecedentedly powerful tool (that has as yet been little used) for studying photoconductivity, photo-Hall effect, luminescence, and other properties of very weakly photoconductive materials, such as ruby and sapphire. Progress in controlling optical damage may be anticipated from knowledge gained from such studies in the future.

APPENDIX

Role of Photo-Electrons in Optical Damage[1*]

R. W. Hellwarth

Department of Electrical Engineering
University of Southern California
Los Angeles, California 90007
and
Hughes Research Laboratories
Malibu, California 90265

Previous workers have discussed the possibility that electrons photo-excited into the conduction band of a polar crystal by a high-intensity, short optical pulse may gain enough energy to damage the lattice by initiating an ionizing avalanche. We discuss here other processes by which these conduction electrons may damage the lattice even before they gain enough energy to ionize their surroundings, specializing our calculations to the case of sapphire and ruby. First, we show that the energy that the conduction electrons absorb linearly from the optical beam is deposited almost immediately in the lattice without significant heating of the electrons. At electron densities ($\sim 10^{16}$ cm^{-3}) and optical intensities ($\sim 10^{10}$ W/cm^2) likely to exist at sapphire damage thresholds, this deposited energy is found to be of the order of what one might expect would be required to form a rupturing shock wave. We also show that the photo-excitation of both bound and unbound impurity levels is enhanced by the presence of conduction electrons, so markedly so for the former that the promotion of electrons into the conduction band may be significantly "bootstrapped," thereby increasing the optical absorption. The presence of conduction electrons and excited impurities in the expected numbers is likely to alter the refractive index significantly and affect thereby the focusing (self- or external) of the beam in a complicated way. For the simplest model these nonlinear index contributions would tend to produce repeated focal regions along the beam. Implications of these results for raising damage thresholds are discussed.

Key words: Crystals, electrons, optical damage, photo-absorption, photo-conductivity, photo-electrons, polar crystals, ruby, sapphire, self-focusing.

1. Introduction

The physical processes responsible for the bulk damage caused in various transparent crystals by short optical pulses (causing negligible electrostriction) have not yet all been identified. Here we argue that several processes not considered previously are likely to be important in the optical damage of inclusion-free polar crystals, especially sapphire and ruby. For their initiation, these processes would all seem to require on the order of 10^{16} conduction electrons per cc to be present at the point of maximum optical intensity, a number widely suspected to be present in sapphire and ruby at peak intensities $\sim 10^{10}$ W/cm^2 just below damage threshold. We will argue here that such densities of cold electrons can a) transfer damaging amounts of heat from the beam to the lattice; b) accelerate the rates of photo-excitation of bound and free impurity electron states, thus significantly increasing the supply of conduction electrons, possibly even in "avalanche"; and c) significantly change the local refractive index, possibly in a way which, in conjunction with the normal nonlinear index, could cause repeated beam focusing along its axis. In none of these processes do the electrons become hot enough (~ 8 eV) to ionize the lattice, in contradistinction to the process suggested by previous workers [1-4][2].

[1] Work supported in part by the Joint Services Electronics Program (U. S. Army, Navy, and Air Force), under Grant No. AF-AFOSR-69-1622A, and in part by the Advanced Research Projects Agency through Air Force Cambridge Research Laboratories.

[2] Figures in brackets indicate the literature references at the end of this paper.

[*] Presented at the ASTM Symposium on Laser Damage, Boulder, Colorado, 24-25 June 1970 and will be published in the Proceedings.

Hence, we will refer to them as "cold" conduction electrons. How the damage processes discussed here depend on crystal temperature, optical wavelength and pulse duration is a complex function of the energies and wavefunctions of the states of the impurities supplying and trapping conduction electrons, the electrons' effective mass(es), the longitudinal optical (LO) phonon structure, and the electron-phonon coupling. Although only the latter two are fairly well known for ruby and sapphire, plausible hypotheses about the former lead one to single out the processes we propose as potentially important to damage. It would appear that reducing donor concentrations or increasing their electron binding energies might produce more damage-resistant crystals. However, if the conduction electron density were proportional to optical intensity (which appears not to be the case at such high intensities), it would tend to reduce self-focusing (or produce a net defocusing) and thereby lower damage thresholds. Other conclusions and suggested experimental checks of electron processes are mentioned in the final Section. In the following Section 2 we summarize the parameters and physical regimes we encounter in ruby and sapphire and we outline our rough criteria for when damage is expected. In Section 3 we define the approach we take for evaluating the required parameters and discuss difficulties with previous calculations of the conditions under which hot ionizing electrons might be produced. The calculations of the enhancement by conduction electrons of lattice heating and photo-excitation follow in Sections 4 and 5. Before proceeding, we first summarize our assessment of often-conflicting reports on photoconductivity in ruby and sapphire.

Hochuli [5] has measured the low-frequency photoconductivity at various wavelengths and temperatures of ruby and sapphire at optical intensities $1 \sim 0.2$ to 5 W/cm^2 and using applied voltages at frequencies zero Hz, 100 Hz, and 9.39 GHz. He found no essential differences in results for the two crystals. The observed conductivities (at 5 W/cm^2) were 4×10^{-13}, 10^{-11}, and 4.2×10^{-8} (6m)$^{-1}$, respectively, at the above frequencies. Since all these frequencies are well below the electron collision frequency (which from the theory of Section 4 we estimate to be $\sim 10^{14}$ rps), the wide variations in results indicate the magnitude of experimental pitfalls in any attempt to measure such low bulk conductivities. Anomalies at the two lower frequencies probably arise from surface effects, from the inability of electric contacts to inject charges into the crystal, and from space charge buildup. Therefore, the 9.39 GHz value, obtained in a microwave cavity with a small electron drift excursion amplitude (of the order of an Angstrom), is probably the most reliable. This conductivity was linear in the optical intensity within the range of observations. Its wavelength dependence suggested that the electrons were supplied from donor levels between 0.6 and 1.2 eV below the conduction band, in agreement with what one would conclude by studying the normal bulk conductivity variation with temperature at higher temperatures. The wavelength dependence also suggested more donor levels appearing around 3 eV. Although Hochuli was able to observe a Hall voltage, it did not vary when the light was turned on or off. The nominal Hall mobility value $\mu = 0.052$ cm^2/V sec. derived therefrom has nevertheless been used without question by other workers whenever a value was required in calculations. This value corresponds to a collision time τ of 4×10^{-17} sec., or an electron mean path of the order 10^{-10} cm, and must be considered unphysical, corroborating the difficulty of making electrodes on sapphire. Using the standard Frohlich theory of a conduction electron in a polar crystal adapted to the large coupling constant of sapphire [6], one estimates τ (at room temperature) to be between $10^{-14.4}$ and $10^{-13.4}$ sec, depending on where the effective band mass lies between 1/10 and 1/2 electron masses. Assuming a free electron mass for which $\tau = 7 \times 10^{-15}$ sec (and $\mu = 12$ cm^2/V sec), one would infer from Hochuli's microwave observations that he produced $\sim 2 \times 10^8$ photo-electrons per cc with 5 W/cm^2 of broadband UV lamp exciting intensity. We see from this that 10^{16} electrons per cc would very likely be excited near damage thresholds of 10^{10} W/cm^2 provided that 10^{16} donor levels per cc were occupied, a provision which is unknown.

Except possibly for the experiments of Belikova, et al. [7, 8], other reported observations of photoconductivity in ruby appear to be plagued by surface and contact effects. Belikova, et al., observed the photoconductivity to be highly nonlinear with the (6943 Å) optical intensity I for intensities near 10^{10} W/cm^2 [7]. One can use our value of τ above with their data to estimate very crudely (since their beam geometry was unspecified) that they were observing well over 10^{16} electrons/cc at 10^{10} W/cm^2 (provided that the electron recombination time was short compared with the optical pulse length). Belikova, et al., also observed optical emission bands near 2, 2.7, and 3 eV (they could not see below 2 eV) which are suggestive of some impurity level transitions. The foregoing is about all one can conclude about photo-electrons from existing data for ruby and sapphire.

2 Description of Electron Interactions

In studying the role of photo-excited electrons in crystal damage, we will constantly apply our formulae to the case of sapphire and ruby. The phonon structure of these two crystals are essentially identical, as are the low-intensity photoconductivities. Although distinct differences in damage behavior have been observed, the gross damage thresholds are statistically indistinguishable for sapphire and ruby. Therefore, most pertinent aspects of these two crystals can be studied together. For brevity, we shall refer hereafter only to sapphire, but shall intend our remarks to apply also to ruby unless stated otherwise. We shall also assume throughout that the optical beam wavelength is 6943 Å, that of the room temperature ruby laser.

A free electron gas of density 10^{16} cm^{-3} has a plasma frequency $\omega_p \sim 6 \times 10^{12}$ rps that is much lower than a) the optical beam frequency of interest ν (2.71×10^{15} rps), b) the phonon frequencies ω_k ($\sim 10^{14}$ rps), and c) typical electronic excitation frequencies ($\sim 10^{16}$ rps).

We shall call a conduction electron "cold" when its energy is much less than interband energies and its wavelength is much longer than the scale of potential variations of the field lattice. Other electrons we will refer to as "hot." The time for cold electrons in the 1/40 to 3 volt range to equilibriate among each other by collisions at a density 10^{16} cm^{-3} is of the order of 10^{-10} to 10^{-13} sec [9], much longer than the inverse electron-lattice collision time ($\sim 10^{-14}$ sec in ruby). Therefore, at least before any large ionizing avalanche occurs, the cold conduction electrons may be studied as independent particles, not interacting among themselves but interacting only with the fields and other particles in the crystal.

When a cold electron moves in a polar crystal such as ruby or sapphire, it is often called a "polaron." Its interactions with the crystal phonons are known to be well-described at room temperature and above by the Hamiltonian derived by Frohlich [10] and used by all previous workers in calculating electron motions leading to damage:

$$H_F = h_o + v_F \tag{1}$$

where

$$h_o = \tfrac{1}{2}[\underset{\sim}{p} - \underset{\sim}{A}(t)]^2 + \Sigma_{\underset{\sim}{k}} \omega_{\underset{\sim}{k}} a^{\dagger}_{\underset{\sim}{k}} a_{\underset{\sim}{k}} \tag{2a}$$

and

$$v_F = \Sigma_{\underset{\sim}{k}} C_{\underset{\sim}{k}} a_{\underset{\sim}{k}} e^{i\underset{\sim}{k}\cdot\underset{\sim}{x}} + \text{h.c.} \tag{2b}$$

Here $\underset{\sim}{p}$ is the electron's momentum, and $\underset{\sim}{x}$ the electron's position coordinates, $a_{\underset{\sim}{k}}$ is the annihilation operation for a LO phonon of frequency $\omega_{\underset{\sim}{k}}$. Optical wavelengths are long enough so that the vector potential $\underset{\sim}{A}(t)$ may be taken as a function of time only oscillating at a frequency ν. We use dimensionless "polaron" units in which the effective band mass of the electron m_b is unity as is Planck's constant $\hbar$. All energies are measured in units of an effective LO phonon energy $\hbar\omega_o$ (680 cm^{-1} or 980° K for sapphire and ruby). Frequencies are measured in units of ω_o ($= 1.6 \times 10^{14}$ rps) so that $\nu = 17$ for a 6943 Å beam in sapphire. Lengths are measured in units of $(\hbar/m_b\omega_o)^{\frac{1}{2}}$ which is 8.5×10^{-8} cm for ruby if we take m_b to be the free electron mass m_o. Frohlich showed that in these units the coupling coefficients $C_{\underset{\sim}{k}}$ are well approximated by $V^{-\frac{1}{2}}(3/4\pi)^{1/2}\alpha\, k^{-1}$ where V is the crystal volume, α is the dimensionless polaron coupling constant $(\epsilon^{-1} - \epsilon_o^{-1})$ (Ryd'/$\hbar\omega_o$)$^{\frac{1}{2}}$. Here Ryd' is the Rydberg for an electron with mass m_o, and ϵ and ϵ_o are the optical and static dielectric constants (3.1 and 10). For $m_b = m_o$, $\alpha \sim 3$ for ruby. In ruby an electron is not if k is of order 10 or more (in polaron units). Hot conduction electrons have neither the simple forms of kinetic energy or lattice interaction energies found in eq (1) but obey complex equations in which exchange must be accounted for and which have never satisfactorily been approximated in usable form for a dynamic lattice. There would seem to be no way at present to make a reliable estimate of how strong an optical field would be required to produce enough interband electronic transitions (i.e., lattice ionization) to cause damage.

From the discussion of the previous section, it is evident that the electrons photo-excited (below damage thresholds) in ruby and sapphire crystals come from donor impurities to which they are bound initially with much less energy than the valence-conduction band gap energy (~ 8 eV). The effects of these impurities on the supply and motions of conduction electrons, as well as on the excitation of the donors by conduction electrons, can be studied by considering the Coulomb interactions v_i between a conduction electron at $\underset{\sim}{x}$ and the i^{th} particle of the α^{th} impurity having charge eq_i^{α} and located at $\underset{\sim}{r}_i^{\alpha}$.

$$v_i = e^2 \epsilon_s^{-1} \sum_{i,\alpha} q_i^{\alpha} / |\underset{\sim}{x} - \underset{\sim}{r}_i^{\alpha}| \tag{3}$$

where the electronic charge e is 4 in our polaron units, and is screened by the dielectric constant ϵ_s appropriate to the frequencies of motions under consideration.

To deal with the elastic scattering of the electrons, one needs only the matrix element of eq (3) diagonal in the impurity's ground state. This gives an effective classical scattering potential seen by the conduction electron. To study inelastic scattering, we will assume that the impurities may be described by an unperturbed Hamiltonian $h_i = \Sigma_\alpha h_{i\alpha}$ with "ionized" or unbound as well as bound electronic eigenstates. Calculations will therefore start from a total Hamiltonian H comprised of

Frohlich's Hamiltonian eq (1) (which describes cold electrons, phonons, and their interactions) plus the electron-impurity interactions of eq (2) and with h_i determining impurity states

$$H = h_0 + h_i + v_p + v_i \tag{4}$$

We will assume that damage to the crystal occurs when the interactions v_p and v_i combined cause the conduction electrons to absorb an energy U per cubic centimeter with a short optical pulse that exceeds a threshold value U_0. That is, we shall strive to determine at what optical beam intensity we may expect

$$U \geq U_0 \tag{5}$$

Present evidence indicates that U_0 is of order 10^2 to 10^3 eV cm^{-3} for ruby and sapphire for 20 nsec pulses in a beam of order one mm diameter. A shock wave of this energy surrounding the beam would develop stresses on the order of the static yield stress [5]. Obviously a large part of understanding optical damage in crystals will be development of an accurate theory of the amount of energy deposition required to produce catastrophic strains as a function of the amount and spatial and temporal distribution of this deposition. However, we shall content ourselves here with the above crude estimate for U_0.

3. Approaches to the Calculation of Damage Thresholds

Previous treatments of the role of electrons in damage [1,4] started from Frohlich's Hamiltonian eq (1) and sought to calculate the optical intensity at which electrons would gain enough energy u to excite an avalanche of interband transitions. The expected energy u of an electron in the optical field was estimated from the equation

$$\frac{du}{dt} = R_{fe} - R_{el} \tag{6}$$

where R_{fe} is the average rate at which the optical field does work on the electron and R_{el} is the average rate at which the excited electron radiates phonons, i.e., transfers its energy to the lattice. Previous treatments have all taken for R_{fe} the usual linear conductivity loss per electron with reasonable order of magnitude estimates from eq (1) for the optical conductivity for electron collision rate. However, they have made approximations for, or statements about, R_{el} that are not directly based on a quantum average of the appropriate operator. Wasserman [1] took for R_{el} the rate at which an electron having a Maxwellian distribution would lose energy to a cooler lattice in the absence of the optical field [A. Gold, Phys. Rev. 110, 76 (1958)]. He predicted breakdown intensities orders of magnitude above those actually observed. Sparks, et al [4], used for R_{el} the approximate rate at which an electron would lose energy to the lattice starting from a momentum eigenstate $|p'\rangle$ for which $\frac{1}{2}p'^2 = u$ also in the absence of the optical field. His predicted thresholds also exceeded observed thresholds by over two orders of magnitude. As a result it is quite probable that a precise evaluation of the spectral energy distribution of an electron obeying eq (1) would show that the electrons do in fact remain too cool to ionize impurities or the lattice at optical fields below damage thresholds. In the next section we show that, indeed, collisions with phonons dominate an electron's motion. We have checked that it follows rigorously from eq (1) that, to lowest order in the optical intensity and coupling parameter α, an electron's expected kinetic energy is simply the sum of its coherently oscillating energy plus $\frac{1}{2}kT$, where T is the ambient lattice temperature. The coherent energy is very much smaller than kT for optical intensities of interest. Therefore, we now proceed to examine whether cold electrons may not mediate the deposition of damaging amounts of energy in a sapphire lattice.

As we mentioned in the previous section, our approach will be to calculate the beam intensity at which the energy U deposited per unit volume in the lattice from the optical field via the electrons exceeds a threshold value U_0. If the maximum optical beam energy per unit area is S, then

$$U = \kappa_\nu S \tag{7}$$

where κ_ν is the absorption per unit length of an optical beam of frequency ν. Following Fröhlich [6], we write the quantum expectation value of the amplitude of an electron's coordinate at frequency ν as $\mathrm{Re}\, E e^{i\nu t}/(m\omega_\nu^2)$ when the electron is in an optical electric field $\mathrm{Re}\, E e^{i\nu t}$. With this definition we have

$$\alpha_\nu \lambda = (\omega_p^2 / c)\, \mathrm{Im}(\nu^2 - \chi_\nu)^{-1} \qquad (8)$$

where λ is the wavelength of the light in the crystal $= 2\pi$ and ω_p is the electron plasma frequency (in units of ω_0). In cgs units $\omega_p^2 = 4\pi e^2 / m_b$ with ρ being the number density of electrons.

The evaluation of α_ν falls naturally into two parts: first, the determination of the rate at which a single conduction electron takes energy from the field (and delivers it to the lattice) by a calculation of χ_ν, and second, the estimation of the number density ρ of these electrons. We consider these two questions, respectively, in the following two sections.

4. Optical Response of Single Electron

We examine first an electron's optical response in the case that it is affected only by electron-phonon interactions as described by Frohlich's Hamiltonian eq (1) with coupling parameters appropriate to sapphire. We then find that, at least at room temperatures and above, collisions with impurities are relatively less important. When the electron response is linear in the applied field for a given lattice temperature, we may use the determination of χ_ν by FHIP who calculated the quantum expected value of the electron motion to first order in the optical field. Their expression is exact for all temperatures at small coupling ($\alpha < 1$) and gives an accurate solution even when $\alpha \sim 3$ as for ruby. In this case it shows that, for $\nu = 17$, both the real and imaginary parts of χ_ν are much less than ν^2 so that we need only calculate $\mathrm{Im}\,\chi_\nu$ to estimate the absorption constant. (The $\mathrm{Re}\,\chi_\nu$ can of course be determined from $\mathrm{Im}\,\chi_\nu$ by Kramers-Kronig relations.)

$$\mathrm{Im}\,\chi_\nu = \frac{2\alpha e^{-\frac{1}{2}\beta}\beta^{3/2}}{3\sinh(\beta\nu/2)} \left(\frac{v}{w}\right)^3 \int_0^\infty \frac{\cos(\nu u)\cos u\, du}{[u^2 + a^2 - b\cos(vu)]^{3/2}} \qquad (9)$$

Here v and w are parameters to be chosen from a variational principle. $a^2 = \beta^2/4 + R\beta\coth(\beta v/2)$; $R = (v^2 - w^2)/(w^2 v)$; and $b = R\beta\sinh(\beta v/2)$.

In the weak coupling limit $v = w = 3$, $R = b = 0$ and $a = \beta/2$. Then the integral can be evaluated exactly in terms of modified Bessel functions. At temperatures much lower than the Debye temperature (β large) this result reduces to

$$\mathrm{Im}\,\chi_\nu \sim 2\alpha(\nu - 1)^{\frac{1}{2}}/3 : \alpha < 1,\ \beta >> 1,\ \nu > 1. \qquad (10)$$

For $\alpha = 3$ and $\nu = 17$, this is 8. The leading correction to eq (10) for finite temperatures multiplies it by $(1 + \beta^{-1})$, increasing it by 30% at room temperature ($\beta = 3.3$).

When $\alpha = 3$, the variational principle gives $v = 3.4$ and $w = 2.55$ in the zero temperature limit [6]. Using these parameters with $\beta = 3.3$ gives $R = 0.220$, $a = 1.866$ and $b = 5.53 \times 10^{-3}$. We have evaluated eq (9) numerically for these parameters and have obtained $\mathrm{Im}\,\chi_\nu = 15$. We have also evaluated eq (9) at frequencies in the neighborhood of $\nu = 17$ and found that, as in eq (10), $\mathrm{Im}\,\chi_\nu$ varies slowly with ν. Therefore, electron transients associated with the rise and fall of even picosecond optical pulses are very small, and it is a good approximation in practice to assume that at any instant the electron's motion is the same as for a purely sinusoidal field of amplitude appropriate to the intensity at that instant. The fast response of the electron's motion, as evidenced by the nonresonant character of χ_ν, together with the knowledge that, at intensities of interest, the electron is gaining negligible energy (staying "cold"), implies that the absorbed energy is being passed on essentially instantaneously to the phonons via the coupling eq (2b). Therefore, it is valid to obtain the rate of deposition of energy in the lattice by determining the rate at which the electrons absorb energy from the optical beam, and we return to this problem.

When a room temperature correction is made to v and w, we guess that, as for small α, the result is raised by around 30% so that the Frohlich model may be taken to yield

$$\mathrm{Im}\,\chi_\nu \sim 20 \qquad (11)$$

for a ruby laser beam driving an electron of band mass equal to a free electron mass in ruby or sapphire at room temperature. The main uncertainty in eq (11) comes from the uncertainty in the effective band mass m_b. $\mathrm{Im}\,\chi_\nu$ varies roughly as $m_b^{3/2}$.

If the temperature goes higher than the phonon energy but is still small compared with ν, then eq (9) yields

$$\mathrm{Im}\,\chi_\nu \to 4a\,\nu^{1/2}/(3\beta) \quad ; \quad a << 1,\ 1 << \beta^{-1} << \nu, \tag{12}$$

showing that the heated lattice causes the electrons to absorb even more light. Note that the "Q" of the electron's oscillation, $\nu^2/(2\,\mathrm{Im}\,\chi_\nu)$, is of order 7 for our estimate eq (11), showing that indeed the optical frequency is much larger than the effective electron collision frequency as we assumed.

One can see at this point that absorption by conduction electrons may cause damage, for, if the electron density were 10^{16} cm^{-3} at an optical intensity of 10^{10} W/cm^2 (which the evidence outlined in Section I suggests as a conservative estimate), and if eq (11) were valid, then $\omega_p^2 \sim 10^{-1}$ and eq (8) gives $\alpha_\nu \sim 0.012$ cm^{-1}. For a 30 nsec pulse this absorption would deposit 40 J per cc in the lattice, somewhat less than the value U_o expected to cause damage. However, Belikova, et al. [7], gave convincing evidence that the electron density is increasing very rapidly with optical intensity at these levels, an occurrence which we expect for reasons given in the following section. Before considering factors which affect the electron density, however, we consider contributions other than those of the linear response eq (9) to electron damping.

First, the question arises as to whether there are significant intensity-dependent corrections to the electron response at the optical frequency as represented by eq (9). (Responses at harmonic frequency multiples do not contribute to the average work done by the optical field on the electrons and so we need not consider these here.) There are two types of nonlinear corrections to eq (9): first, those arising from the nonlinear reactions of the phonons on the electron, and, second, those arising from the intensity-dependent deviations of the momentum distribution of electrons from a thermal distribution. We have estimated both effects by expanding the quantum expression for the expected electron position (and velocity) to the third order in the electric field. We have found that both effects tend to diminish the optical absorption from its linear response value, a result expected on the physical grounds that electrons of high energy interact less with the optical phonons than do low-energy electrons. For both corrections the natural dimensionless expansion parameter is $(k_o r_o)^2$ where k_o is the wavevector of an electron having energy $\frac{1}{2}\nu$ and r_o is the classical amplitude of a free electron oscillating in the applied optical field. In our case this parameter is $\sim I(\mathrm{W/cm^2}) \times 10^{-13}$. Since optical intensities have not yet been observed to approach even 10^{11} W/cm^2 before damage, we conclude that the nonlinear corrections to eq (9) are too small to be of importance in present considerations.

Next, we see why, under conditions of interest here, phonon scattering of conduction electrons dominates scattering by ionized and un-ionized lattice impurities. For each conduction electron there is in the lattice a heavy positive ion whose charge is shielded roughly by the static dielectric constant of the lattice ($\epsilon_o \sim 10$). The linear absorption by 10^{16} electrons per cc in such a two-component plasma at room temperature is $\sim 10^{-6}$ per cm [11]. This is so small compared with phonon effects that one can readily appreciate that even if 10^{19} per cm^3 of electrically neutral scattering centers were added to the lattice, one would not expect them to scatter electrons as effectively as do phonons at room temperature and above. This predominance of phonon scattering at or above room temperature has been observed in various ways even in crystals whose electron-phonon coupling is much smaller than in ruby and sapphire [12]. Having estimated the optical response of a single conduction electron, we now proceed to consider how their numbers are affected by their interactions with lattice impurities.

5. Conduction Electron Interactions with Impurities

From incomplete existing absorption [13] and luminescence [8] data, it is evident that sapphire has a complex impurity level structure with energy differences ranging up to at least 3 eV. Light of any single optical wavelength, such as 6943 Å, will not be resonant with a significant fraction of the bound-bound transitions and, of course, will only excite transitions to the conduction band from bound levels within 1.8 eV of the band edge. If, however, the light became effective in exciting a large fraction of the bound-bound transitions, then cascade transitions of electrons into the conduction band from levels lying more than 1.8 eV below the band edge might dominate direct photo-excitation. We shall now show that, at conduction electron densities $\sim 10^{16}$ cm^{-3}, the light does become so effective in exciting bound-bound transitions with which it is <u>not</u> resonant that cascade photo-excitation may become important in increasing the conduction electron density near optical damage intensities. These non-resonant transitions are possible because the conduction electrons readily absorb the difference in energy $\nu - \omega_{ba}$ between an absorbed photon and the energy of transition between the upper and lower states $|b\rangle$ and $|a\rangle$. We now show that the rate R_{ab} for a typical impurity to make such a transition, multiplied by a reasonable impurity density ($\sim 10^{19}$ cm^{-3}), may exceed the total direct photo-excitation rate, and thereby initiate cascade ionization of impurities.

To calculate the rates R_{ab} it is convenient to re-express the interaction of eq (3) as a Fourier transform (the impurity index a is now omitted since we are considering only one impurity):

$$v_t = \sum_{\underset{\sim}{k}} v_{\underset{\sim}{k}} e^{i\underset{\sim}{k}\cdot\underset{\sim}{x}} \tag{13}$$

where $v_{\underset{\sim}{k}}$ is the impurity operator $4\pi e^2 V^{-1} \epsilon_s^{-1} k^{-2} \Sigma_j \exp i\underset{\sim}{k}\cdot\underset{\sim}{r}_j$ and V is a fiducial interaction volume. The sum is confined to the bound impurity electrons as only electronic transitions will be considered. For the transitions of interest we may take ϵ_s to be the optical dielectric constant ϵ. With the form eq (13) it is a straightforward matter to re-derive the quantum "Golden Rule" for calculating transition rates but with an unperturbed Hamiltonian $h_o = \frac{1}{2}(\underset{\sim}{p} - \underset{\sim}{A}_o \cos\upsilon t)^2$ instead of $\frac{1}{2}p^2$. To lowest order in the electron-impurity interaction, the rate for an electron to scatter from momentum state $|\underset{\sim}{p}\rangle$ to $|\underset{\sim}{p} + \underset{\sim}{k}\rangle$ while the impurity goes from $|a\rangle$ to $|b\rangle$ is

$$\Gamma(\underset{\sim}{p} \to \underset{\sim}{p} + \underset{\sim}{k};\ a \to b) = 2\pi\, |\langle b| v_{\underset{\sim}{k}} |a\rangle|^2 \sum_{n=-\infty}^{\infty} \delta(k^2/2 + \underset{\sim}{p}\cdot\underset{\sim}{k} + \omega_{ba} + n\upsilon) \cdot [J_n(\underset{\sim}{k}\cdot\underset{\sim}{r}_o)]^2 \tag{14}$$

where we have retained the terms for n-photon emission and absorption for future comparison with the $n = 1$ term that we are now considering. In the polaron units used here the classical electron oscillation amplitude r_o equals E/υ^2, where the real amplitude E of the optical electric field equals the amplitude in esu divided by $E_o = (\omega_o^2/e)(\hbar m_b/\omega_o)^{\frac{1}{2}}$. For our parameters E equals (the field in V/cm) $\div$ (1.24×10^6). The Bessel function coefficients J_n in eq (14) are the exact amplitudes for absorbing (or emitting) n optical photons in the process. Their arguments are of order $10^{-13}\, I(W/cm^2)$ and so the approximation $J_n(x) \sim (x/2)^n/n!$ is accurate here. Consider now the rate r_{ab} for the impurity interacting with one electron in the optical field to make a transition from a state $|a\rangle$ to a state $|b\rangle$, for which $\omega_{ba} < \upsilon$. In terms of the rate eq (14)

$$r_{ab} = \sum_{\underset{\sim}{p},\underset{\sim}{k}} f(\underset{\sim}{p})\, \Gamma(\underset{\sim}{p} \to \underset{\sim}{p} + \underset{\sim}{k};\ a \to b) \tag{15}$$

where f(p) is the initial conduction electron distribution and only the $n = 1$ term in Γ is needed. To evaluate r_{ab} it remains to estimate the dependence of the matrix elements of $v_{\underset{\sim}{k}}$ on $\underset{\sim}{k}$. We shall use the "dipole approximation" in which $\langle b|\exp i\underset{\sim}{k}\cdot\underset{\sim}{r}_j|a\rangle \sim i\underset{\sim}{k}\cdot\langle b|\underset{\sim}{r}_j|a\rangle$. For definiteness we will assume that the impurity is spherically symmetric so that $|\Sigma_j \underset{\sim}{k}\cdot\langle b|\underset{\sim}{r}_j|a\rangle|^2 = k^2 X_{ba}^2$ where X_{ba} is the dipole matrix element of the impurity transition. Finally, before evaluating eq (20), we average over all directions of $\underset{\sim}{E}$ so that the J_1^2 terms becomes $(kE/2\upsilon)^2/3$. The $n = 1$ contribution to the sum over $\underset{\sim}{k}$ in eq (15) is then

$$r_{ab} = V^{-1}\, 16\pi\, e^4 (r_o^2/12)\, c^{-2}\, X_{ab}^2 \sum_p L(p)\, f(p) \tag{16a}$$

where

$$L(p) = \int_{K_m - p}^{K_m + p} dk\, k^{2n-1}/p. \tag{16b}$$

Generally $K_m \approx [p^2 + 2(\upsilon - \omega_{ba})]^{\frac{1}{2}}$ is much larger than the magnitude of p allowed in f(p). In this case, it is sufficiently accurate to approximate eq (16b) by

$$L \sim 2[2(\upsilon - \omega_{ba})]^{\frac{1}{2}} \tag{17}$$

and we see that the impurity excitation rate is essentially independent of the initial small conduction electron momentum p. Since $\Sigma_p f(p) = 1$, this fact makes the sum in eq (16a) trivial. The total rate R_{ab} for an impurity to absorb a photon is r_{ab} times the number of conduction electrons in the interaction volume V. It is convenient to express R_{ab} in terms of a photon absorption cross-section σ_{ab} which equals $R_{ab} \div$ (the incident photon flux). Recalling that $2\upsilon\, r_o^2$ is numerically $10^{-13}\, I(W/cm^2)$, we have from eq (15) for sapphire

$$\sigma_{ab} \sim 7.5 \times 10^{-11}\, I\, X_{ab}^2\, c^{-2}\, \upsilon^{-1} (\upsilon - \omega_{ba})^{\frac{1}{2}}\, \rho_e \tag{18}$$

in polaron units where the electron density ρ_e is 6.15×10^{-22} times the number of electrons per cc ρ.

To see the importance of the transition cross-section eq (18) relative to direct photo-excitation, we estimate the density of impurities N_i cm^{-3} that would be required to attenuate the optical beam more than does the direct photo-excitation process. Of course, the latter attenuation is not known, but it must be less than the total attenuation in sapphire, and that is less than 10^{-2} per cm. For argument, suppose that direct photo-excitation causes less than 10^{-3} per cm optical attenuation (it probably causes much less). For our estimate, let us assume in eq (18) that $X^2_{ab} \sim 1/\omega_{ab}$, $\omega_{ab} \sim 8$, and $I = 10^{10}$ W/cm^2 and $\tau = 10^{10}$ as in previous examples. This gives $\sigma_{ab} \sim 10^{22}$ cm^2 so that $N_i \sim 10^{19}$ impurities per cc would be required to make these conduction-electron-mediated impurity transitions attenuate the optical beam by 10^{-3} per cm. Considering all the kinds of dislocations and foreign ions which might take part as impurities in this process, we feel that it is not unreasonable that such an impurity density could exist. Of course, there are so many order-of-magnitude estimates of unknown quantities in the foregoing that the result can only be considered as suggestive of a kind of process that must be considered as competitive with other possibilities at this time. However, the experimental observation of a rapidly increasing dc photoconductivity near damage thresholds [7] does suggest a "bootstrap" process such as the above by which conduction electrons can create more of their kind, even before they become so energetic as to ionize the lattice.

We have examined the enhancement of the single-photon bound-free photo-excitation transitions that arise from eq (14), and have estimated that excitation cross-section also to be of order 10^{-22} cm^2 under the same conditions. This is probably less than the cross-section for direct photo-excitation. If multi-photon excitation is important in producing electrons, then the higher n terms of eq (14) probably dominate direct absorption near damage levels. The expansion parameter in eq (14) is of order 10^{-13} I(W/cm^2), whereas it is $\sim 10^{-17}$ I for direct multi-photon absorption.

6. Focusing Effects

In a region of the crystal in which conduction electrons have been excited there is a change in the refractive index δn given by

$$\delta n = -\omega_p^2/\nu^2 . \tag{19}$$

At a density 10^{16} cm^{-3}, electrons (with free electron band mass) have a plasma frequency of 10^{12} Hz, which gives $\omega_p/\nu \sim 0.0023$ and $\delta n \sim 5.3 \times 10^{-6}$. This index change is comparable to that required to self-focus a one milliradian gaussian beam. If the electron density were proportional to the optical intensity I, and this index change were produced when I = 10^{10} W/cm^2, then the index change would constitute a second order nonlinear index (often written $n_2 \overline{E^2}$) whose nonlinear coefficient n_2 would be -2×10^{-13} esu. This is negative and an order of magnitude larger than what one would guess is the intrinsic nonlinear index of the bound electrons in sapphire. However, we suspect that the electron density is increasing much more rapidly than I at high intensities [7] and so the effect of the index of eq (19) is not simple. Furthermore, impurity electrons which are excited to bound states more than $\hbar\omega$ below the band edge, such as by the process discussed in the previous section, have an increased polarizability and would tend to cancel the effect eq (19) of conduction electrons.

Suppose the net effect of impurity transitions were to produce a negative and highly nonlinear refractive index change, as would be the case if the conduction electron effect eq (19) dominated. Then there would be strong self-defocusing of a beam in regions of very high intensity, but only the intrinsic self-focusing index would be operative in regions of smaller intensity. This would evidently result in successive regions of high intensity along the beam as each effect produces in turn a focusing tendency that brings the other effect into dominance. Damage tracks in sapphire and other materials consist of a sequence of damage bubbles that are suggestive of such a process. However, we have not calculated the spacing of the successive high-intensity regions on the basis of some reasonable model to see whether there is any possible correspondence between these speculations and observation.

7. Discussion

Although there are alternate explanations for the behavior of damage tracks observed in sapphire [14], it seems likely that self-focusing is occurring and playing a role in the damage. (It is curious that the appearance, lengths, and positions of damage tracks differ between ruby and sapphire.) If self-focusing is occurring, it makes especially difficult the determination of the actual optical intensity at which the material ruptures, and this in turn lends an extra uncertainty to the parameters we have used in discussing the role of conduction electrons in damage. Probably the most promising way to determine more precisely what the electrons' role may be is to determine the parameters of these conduction electrons below damage intensities. It would be especially desirable to have reliable dc photoconductivity measurements between the intensities 5 W/cm^2, the highest used by Hochuli [7], and 10^{10} W/cm^2, the lowest used by Belikova, et al. [7], in their measurements. With the high light intensities available with lasers, it may now be possible to excite enough electrons to obtain a

meaningful Hall effect. Perhaps the time decay of photoconductivity and luminescence after an exciting pulse could be observed and yield information on carrier lifetimes, trapping times, etc. Unfortunately, the important and pervading parameter – the effective mass in the conduction band (and its anisotropy) – appears to be extremely difficult to determine experimentally.

Should the photo-excited electrons be found to play significant roles in damage, such as those we have discussed, then it may be possible to fabricate more damage-resistant sapphire and ruby. For example, if self-focusing is presently instrumental in damage, then it might be reduced by adding donor impurities that produce a linear photoconductivity at high intensities and thus reduce the total nonlinear index via the index change of eq (19). On the other hand, those donors that give a highly nonlinear photoconductivity and a sudden production of high electron densities that result in rupture by photo-absorption may perhaps be eliminated from the crystals or compensated by other additives. In any case, it is evident that the availability of high-intensity laser sources will greatly facilitate the study of the conduction bands and impurity levels in very weakly photoconducting materials such as sapphire and ruby.

8. References

[1] A. Wasserman, "A mechanism for damage in solids by intense light," Appl. Phys. Letters 10, 132-133 (1967).

[2] V. A. Pashkov and G. M. Zverev, "Destruction of ruby and leucosapphire crystals by strong laser radiation," Soviet Phys. -JETP 24, 516-518 (1967).

[3] E. A. Sviridenkov, "Mechanism of damage of ruby by laser radiation," Soviet Phys. -Solid State 9, 1917-1918 (1968).

[4] G. M. Sverev, T. N. Mikhailova, V. A. Pashkov, and N. M. Solov'eva, "Mechanisms of destruction of ruby and leucosapphire crystals by powerful laser radiation," Soviet Phys. -JETP 26, 1053-1057 (1968).

[5] Urs E. Hochuli, "Photoconductivity in ruby and sapphire," Phys. Rev. 133A, 468-471 (1964).

[6] R. P. Feynman, R. W. Hellwarth, C. K. Iddings, and P. M. Platzman, "Mobility of slow electrons in a polar crystal," Phys. Rev. 127, 1004-1017 (1962). Hereinafter referred to as FHIP.

[7] T. P. Belikova and E. A. Sviridenkov, "Photoconductivity of ruby when strongly irradiated by a ruby laser," JETP Letters 3, 257-259 (1966).

[8] T. P. Belikova, A. N. Savchencko, and E. A. Sviridenkov, "Optic breakdown in ruby and related effects," Soviet Phys. -JETP 27, 19-23 (1968).

[9] L. Spitzer, Jr., Physics of Fully Ionized Gases (Interscience Publishers, New York, 1956).

[10] H. Frohlich, "Theory of electrical breakdown in ionic crystals," Proc. Phys. Soc. (London) A160, 230-241 (1937).

[11] V. I. Perel and G. M. Eliashberg, "Absorption of electromagnetic waves in plasma," Soviet Phys. -JETP 14, 633-637 (1962).

[12] R. H. Bube, Photoconductivity of Solids (John Wiley and Sons, New York, 1960).

[13] N. V. Beardsley, Proceedings of the Infrared Information Symposia, Volume 1, No. 2, 47-53 (1956).

[14] C. R. Giuliano and L. D. Hess, "Laser-induced damage in ruby and sapphire," in these Proceedings.

DOCUMENT CONTROL DATA - R&D

(Security classification of title, body of abstract and indexing annotation must be entered when the overall report is classified)

Aerojet Aircraft Company, Research Labs. Div.
3011 Calibu Canyon Road
Calibu, California 90265

2a. REPORT SECURITY CLASSIFICATION: Unclassified

2b. GROUP

3. REPORT TITLE

DAMAGE THRESHOLD STUDIES IN LASER CRYSTALS: EXPERIMENTAL AND THEORETICAL RESULTS IN RUBY AND SAPPHIRE

4. DESCRIPTIVE NOTES (Type of report and inclusive dates)

Scientific Interim

5. AUTHOR(S) (First name, middle initial, last name)

Concetto R. Giuliano
Robert W. Hellwarth
LaVerne D. Hess
Gerald R. Rickel

6. REPORT DATE: July 1970

7a. TOTAL NO. OF PAGES: 48

7b. NO. OF REFS: 1

8a. CONTRACT OR GRANT NO.: F19628-69-C-0277 ARPA Order No. 1434

8b. PROJECT, TASK, WORK UNIT NO.: 8693-n/a-n/a

8c. DOD ELEMENT: 61101D

8d. DOD SUBELEMENT: n/a

9a. ORIGINATOR'S REPORT NUMBER(S): Semiannual Report No. 2

9b. OTHER REPORT NO(S) (Any other numbers that may be assigned this report): AFCRL-70-0437

10. DISTRIBUTION STATEMENT

1- This document has been approved for public release and sale; its distribution is unlimited.

11. SUPPLEMENTARY NOTES

This research was supported by Advanced Research Projects Agency

12. SPONSORING MILITARY ACTIVITY

AF Cambridge Research Labs (OPL)
L.G. Hanscom Field
Bedford, Massachusetts 01730

13. ABSTRACT

In this report the results of a number of experiments are presented as well as a summary of the theoretical work. Bulk damage thresholds for several ruby and sapphire samples from different sources are presented. The problem of surface damage is discussed, and qualitative comparisons between entrance and exit surface damage are made. Differences between the gross characteristics of bulk damage in ruby and sapphire are presented and discussed. The dependence of damage threshold on TiO_2 doping and optical pumping is presented. The unexpected results are discussed and further experiments proposed. The theoretical treatment deals with processes by which "cold" conduction electrons may damage the lattice before they gain enough energy to ionize their surroundings. It is shown that the energy that the conduction electrons absorb linearly from the optical beam is deposited almost immediately in the lattice and is of sufficient magnitude to form a rupturing shock wave. It is also shown that the photoexcitation of impurity levels is enhanced by the presence of conduction electrons. The presence of conduction electrons and excited impurities is likely to alter the refractive index significantly and affect the focusing (self- or external) in a complicated way. Implications of these results for raising damage thresholds are discussed.

DD FORM 1 NOV 65 1473

UNCLASSIFIED
Security Classification

14. KEY WORDS	LINK A		LINK B		LINK C	
	ROLE	WT	ROLE	WT	ROLE	WT
Bulk damage						
Crystals						
Damage thresholds						
Electrons						
Lasers						
Mode control						
Optical Pumping						
Ruby						
Sapphire						
Self focusing						
Surface damage						